Evaluation of the Operational Mercator global ocean analysis and forecast system modelled current vector product with *in-situ* ADCP data in the Southern Benguela Upwelling System

Emily Gammon
(GMMEMI002)

Department of Biological Sciences
University of Cape Town
Rondebosch, Cape Town
South Africa

Supervisor (s): Dr Barry Clark (Anchor Environmental Consultants)
Kevin Schmidt (Anchor Environmental Consultants)
Prof Marcello Vichi (University of Cape Town)

June 2025

Dissertation submitted in partial fulfilment of the requirements for the degree of Master of Science (by coursework and dissertation) in Applied Ocean Sciences, through the Marine and Antarctic Research centre for Innovation and Sustainability (MARiS), in the Department of Biological Sciences, at the University of Cape Town

Plagiarism Declaration

I, Emily Gammon, hereby:

1. grant the University of Cape Town free license to reproduce the above thesis in whole or in part, for the purpose of research;

2. declare that:

   (a) this dissertation is my own unaided work, both in concept and execution, and apart from the normal guidance from my supervisor, I have received no assistance except as acknowledged.
   (b) neither the substance nor any part of the above dissertation has been submitted in the past, or is being, or is to be submitted for a degree at this University or at any other university.

Signed by candidate

Emily Gammon

Department of Biological Science
University of Cape Town

Sunday 1 June, 2025

Abstract

Global ocean current vector datasets are frequently used to force, or are assimilated into, local and regional particle tracking and pollutant dispersal models, metocean forecasting platforms, climate analyses, and natural resource management applications. The Operational Mercator global ocean analysis and forecast system (Mercator data product), made publicly available in 2022, provides near-real-time vector components of global ocean currents at 50 vertical levels (depths) in the water column with a horizontal resolution of 1/12 degree. Validation of ocean forecasting and simulation models is required to assess a modelled product's ability to represent the local environment. Validation is done using in-situ data such as those gathered by Acoustic Doppler Current Profilers (ADCP). In this study, an upward-facing Nortek Signature 250 ADCP was deployed at a depth of 123 m off the Southern Namibian coast for ten months. The resulting current profile data were used to validate the Mercator data product for the same area. Data collected by the ADCP and simulated data from the NEMO model were matched spatially (nearest-neighbour) and temporally (rolling average), and the similarity of current vector components was statistically investigated. Spearman Rank-Order Correlation, root-mean-square-error and bias were calculated for the full time series. The seasonal percent occurrence of current vector magnitude and direction were subsequently derived to assess the Mercator data product's ability to represent seasonal variability. The Mercator data product captured the seasonal variation in the magnitude of the nearshore southern Benguela Upwelling System for both the zonal and meridional components well. The Mercator data product represented much lower complexity in the direction of bulk flow

within the system but did contain the daily oscillation pattern measured by the ADCP. The Benguela Current is a physically complex eastern boundary current spanning three countries, used extensively for fishing, mining, maritime transit, and oil extraction. The ocean current outputs from the Mercator data product could allow for improved pollution modelling (oil dispersion or plume modelling), improved fuel optimisation models for maritime transit, and productivity prediction to support fisheries management without the cost of deploying devices to measure ocean currents *in situ*.

Keywords: Ocean surface current, Model validation, Benguela Current, Acoustic Doppler Current Profiler

Acknowledgements

I want to express my deepest gratitude to my supervisors, Professor Marcello Vichi, Dr Barry Clark, and Kevin Schmidt for their input, guidance, and support. I would like to thank Anchor Environmental and DeBeers Marine Namibia for providing the *in-situ* ADCP data.

Table of Contents

List of Figures

List of Tables

List of Symbols/Abbreviations

ADCP – Acoustic Doppler Current Profiler

ASCA – Agulhas System Climate Array

CTD – conductivity, temperature, depth

ENSO - El Niño-Southern Oscillation

EOS – Equations of state

GLO12v4 – GLOBAL_ANALYSIS_FORECAST_001_024 version 4

LSB – land-sea breeze

m/s – metres per second

NEMO – nucleus for European modelling of the ocean

NOAA – National Oceanic and Atmospheric Administration

PIRATA – Prediction and Research Moored Array in the Tropical Atlantic

RAMA – Research Moored Array for African-Asian-Australian Monsoon Analysis and Prediction

RMSE – Root-mean-square-error

ROMS – Regional Ocean Modelling System

RS – remote sensing

SAMBA – South Atlantic MOC Basin-wide Array

SD – standard deviation

Sig250 – Nortek Signature 250

SOG – speed over ground

SSH – sea surface height

SST – sea surface temperature

STW – speed through water

TAO/TRITON – Tropical Atmosphere Ocean

U – Zonal (east-west) current component

V – Meridional (north-south) current component

P – Spearman's Rank Correlation

1 Introduction

Ocean currents are large-scale water movements that connect marine ecosystems and influence the global climate. They are measured in many ways and impact the way people interact with the ocean. As humanities understanding of ocean currents has improved, predictive models have been created. These models require validation against real world measurements. The Operation Mercator global ocean physical analysis and forecasting product (Mercator data product) is hosted by Copernicus Marine Data Store and produces subdaily three-dimensional ocean current data for the global ocean. This study uses *in situ* current data collected by an Acoustic Doppler Current Profilers (ADCP) in the southern Benguela Upwelling System. This study intends to assess the ability of the Mercator data product to capture overall trends, variability, and seasonality of the ocean currents in this region.

1.1 Ocean currents and the southern Benguela Upwelling System

The west coast of Southern Africa is host to a unique blend of major ocean currents from three ocean basins. Warm water from the Indian Ocean is transported to the Southern Atlantic in spin-off eddies and filaments from the Agulhas current. Cold waters from the Southern Ocean are transported north by the Benguela Current. Two main mechanisms drive these currents in this area: wind-driven ‘Ekman’ surface currents and pressure driven geostrophic currents (Gross, 1977). Wind energy is transferred to the surface waters and down the water column, dissipating in magnitude with depth (called an Ekman spiral). A phenomenon called the Coriolis effect (which is due to the centrifugal force generated by the Earth’s rotation) results in a gradual

deflection of water slightly to the right in the Northern Hemisphere and the left in the Southern Hemisphere with each layer of water impacted. This results in the net movement of the water mass being 90 degrees to the left or right of the prevailing wind depending on the hemisphere, called Ekman transport. Water movement (wind-driven or tidal) creates a dynamic topography on the ocean surface with areas of lower sea surface height (SSH) and higher SSH. This can be amplified by water masses of different temperatures and salinities that have different densities. Gravity then acts on these differential SSH, drawing the water down pressure gradients. This gravity-driven water movement is once again impacted by the Coriolis force drawing it left or right depending on the hemisphere. The net interaction of gravitational force and Coriolis force means that water parcels tend to move along contours of equal pressure, taking the form of geostrophic currents (Gross, 1977).

The Benguela is the eastern boundary current of the anticyclonic South Atlantic subtropical gyre, running from the Cape Peninsula to southern Angola before deflecting northwest across the Atlantic (Shannon, 2006). It is a complex and dynamic space, with a main current (0.15-0.40 m/s speed) and a nearshore fast-flowing coastal jet (0.25-0.75 m/s speed) moving northward, as well as a returning nearshore seasonal counter current driven by wind-stress and a slope edge poleward undercurrent moving southwards along the continental shelf (Figure 1) (Ragoasha et al., 2019). This area is characterized by strongly seasonal wind-driven upwelling that brings cooler bottom-waters and high nutrient concentrations to the surface, often resulting in phytoplankton blooms (Moloney, 1992; Shannon, 2006). This region is of particular interest due to the important role it plays in food availability, climate regulation, extraction of natural resources and tourism (Hamukuaya, 2020; Kainge et al., 2020).

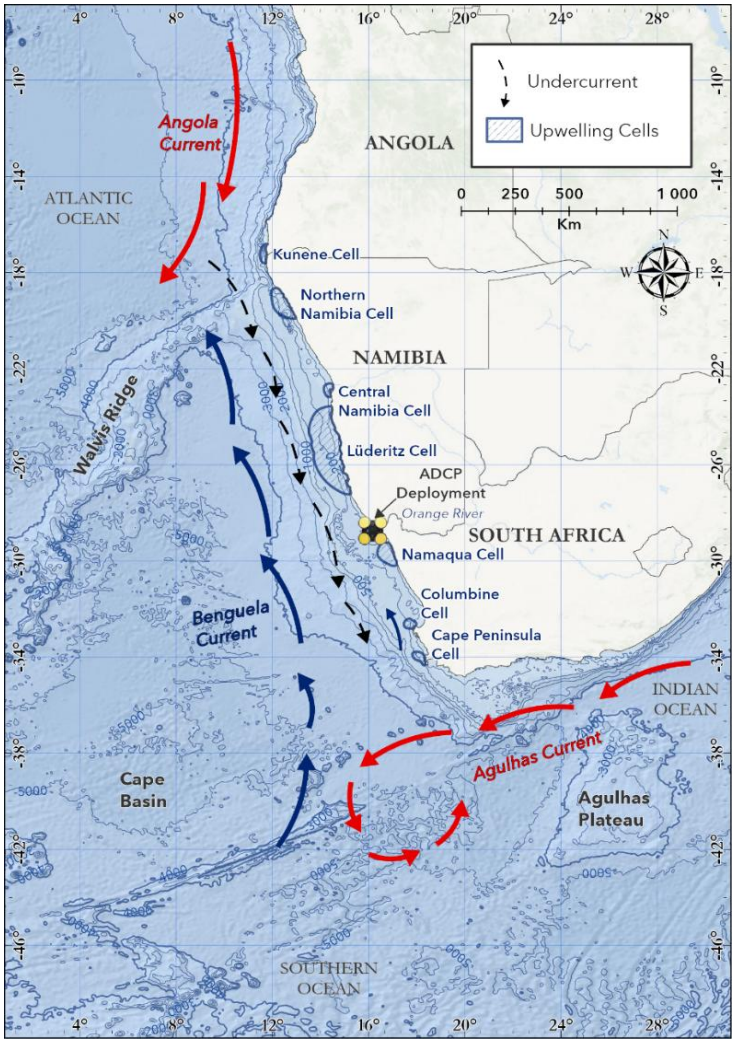

Figure 1. Major bathymetric features, upwelling cells, major current features and flow of the current systems of the western coast of southern Africa.

1.2 The importance of ocean currents

The ocean covers over 70% of the Earth's surface and have been utilised by people for millennia (Erlandson & Fitzpatrick, 2006). The Benguela Upwelling System has many uses and impacts – as a source of food, transportation, natural resources, and recreation. Many environmental factors feed into the efficient and sustainable use of these resources, such as sea surface temperature (SST) and predicting fish shoal locations, ocean dynamics and oil spill clean ups, and ocean currents and fuel

optimization in shipping. This section investigates how our understanding of ocean currents impacts the utilisation of the Benguela Upwelling System.

The global fishing industry lands around 80 million tonnes of fish a year, 88% of which goes towards human consumption, utilised by 7.8 billion people in 2020 (FAO, 2022). The Benguela Upwelling System has a wide variety of commercially important species, from small pelagics like sardine (*Sardinops sagax*) and anchovy *(Engraulis encraicolus*), to hakes (*Merluccius paradoxus* and *M. capensis*), snoek (*Thyrisites atun*), Horse mackerel (*Trachurus capensis*), and Albacore tuna (*Thunnus alalunga*) (Kainge et al., 2020). The locations at which shoaling fish species aggregate are impacted by biophysical features, including SST, chlorophyll concentrations, currents, mixed layer depth, dissolved oxygen, and salinity (Klemas, 2012, 2013; Kacev & Lewison, 2016). Some of these variables are remotely measurable from satellites and are often used to drive models that predict the locations of fish aggregations (Armas, Arancibia & Neira, 2022). Economically valuable species like tuna (Myers, 1990), sardine (Santos & Fiuza, 1992), and mackerel (Grimes, 2001) are associated with strong vorticity and frontal structures linked to upwelling, relaxing, and oceanographic events. Commercial fisheries have been using remotely sensed data to predict and track fish since the mid-1930s when the Japanese government started a fishery forecasting service (mainly focused on SST, but also including other oceanographic conditions) via national radio broadcast (Yamanaka et al., 1988). The National Oceanic and Atmospheric Administrations (NOAA) Fisheries Mississippi Laboratories developed fisheries probability model products in the 1980s, which reduced the search area of the butterfish fishery in the Gulf of Mexico by ~70% (Leming, 1990). A forecasting system for identifying potential fishing zones was developed and validated

in Indian waters that shows a 70-90% success rate in identifying fishing zones 2-3 days in advance (Klemas, 2012). Remotely sensed and modelled ocean current data helps optimize fishing by reducing fuel costs and time at sea and reduce bycatch by predicting distributions of sensitive species and informing dynamic no-take zones.

Maritime transport is economically important to the countries neighbouring the Benguela system in providing connectivity to international markets (Finke et al., 2020). Shipping on an international scale moves more than 80% of the world's trade by volume and contributes billions of tonnes of greenhouse gases each year (approximately 3.1% of global emissions) making it an area of interest for green initiatives (Yang et al., 2020; Wang et al., 2021). Ship voyage optimization is a strategy involving route planning for trajectory and engine power based on weather conditions and ocean currents. It aims to use the ship engine as little as possible and take advantage of the environment while still getting the ship to the appropriate port on time (Yu et al., 2021). The relationship between fuel efficiency and environmental variables is complex, as shown in the difference between speed through water (STW) and speed over ground (SOG), which is mainly due to ocean currents (Yang et al., 2020). Well-performing models of currents in boundary systems like the Benguela could assist maritime transport agencies in planning fuel and time-effective routes in the future.

The Benguela system is host to many marine activities that result in pollution such as fishing, offshore mining, oil/petroleum extraction and transit, ports, tourism, and industrial outfalls (Hamukuaya, 2020). The South Atlantic as a wider system also contains many of these pollution sources (oil rigs, shipping, fisheries, mining) (Hatje et al., 2021). Deep-sea mining produces sediment plumes that impact filter-feeding

species, disrupt bioluminescence, and bury benthic habitats (Washburn et al., 2019). These plumes are often monitored through plume modelling, which requires detailed knowledge of currents in the region through the water column (Spearman et al., 2020). The same is true for dispersal models that track oil spills and industrial outfalls, where data on ocean currents, waves, and winds are crucial for the performance of the models (Keramea et al., 2021). With so many of these activities taking place in this region of the Southeast Atlantic, accurate current simulation models are valuable.

The El Niño-Southern Oscillation (ENSO) is a recurring climate pattern with three states, El Niño (warmer waters), Neutral, and La Niña (cooler waters). It is defined by fluctuations of SST and air pressure in the atmosphere over the equatorial Pacific Ocean, and the relationship that changing SST has with sea-level pressure and the Walker Cells (Lv, Fan & Zhang, 2022; Wang, Cheng, et al., 2023). ENSO has been shown to impact upwelling in the Benguela system, weakening it after an El Niño and strengthening it after a La Niña (Rouault & Tomety, 2022). The ability to track and forecast the stage and onset of the ENSO cycle could help to facilitates a better understanding of its impact on the global climate and therefore has implications for agriculture, fisheries, and ecosystems (Glantz et al., 2022). Tracking and predicting ENSO events can help countries with disaster readiness and resilience (Vigil & Booker, 2023).

1.3 How ocean currents are measured

Ocean currents can be measured with *in-situ* devices, inferred using satellite-derived air-sea interface products, or modelled using a combination of satellite and *in-situ* data.

In-situ measurements provide direct measures of ocean currents and capture a high degree of complexity compared to modelled currents, which have a high spatial and temporal coverage at the cost of resolution and output of fine-scale features (Dohan, Lumpkin & Maximenko, 2014). *In-situ* devices come in three main categories; free-floating drifters, ship-mounted devices, and moored devices. Drifters are loose in the ocean, moving wherever the currents take them at their drifting depth and transmitting their location from the surface to satellites (Laurindo, Mariano & Lumpkin, 2017). Shipboard devices measuring currents are normally mounted Acoustic Doppler Current Profilers (ADCP) (Dohan, Lumpkin & Maximenko, 2014). ADCPs work with acoustic transducers that send pings into the water column and 'listen' to the backscatter off particles in the water column. They operate with at least three sensor heads, using triangulation and the Doppler shift to calculate the movement of the particles in the water and derive water movement from that. Also giving fine granularity but limited spatial coverage are moored current meter (including but not limited to ADCP devices) on single moorings, or mooring arrays. The largest and most internationally collaborative arrays that incorporated ADCPs with other sensors are PIRATA (Prediction and Research Moored Array in the Tropical Atlantic) in the North Atlantic Ocean, RAMA (Research Moored Array for African-Asian-Australian Monsoon Analysis and Prediction) in the Indian Ocean, TAO/TRITON (Tropical Atmosphere Ocean) in the Pacific Ocean, SAMBA (South Atlantic MOC Basin-wide Array) in the southern Atlantic Ocean, and ASCA (Agulhas System Climate Array) across the Agulhas current in the Indian Ocean (Figure 2). These arrays offer long time series of data but require extrapolation between them.

Figure 2. Locations of the largest and most internationally collaborative mooring arrays.

While ocean currents are modelled rather than being directly measured by remote sensing (RS) techniques, these ocean current models require input data like sea level anomalies, SST, and sea ice concentrations that are measured directly, and so a brief explanation of how RS works is provided (Lellouche et al., 2022). RS entails the use of sensors in the atmosphere (on planes or balloons) and in space (on satellites or space shuttles) to gather information about what is happening on the surface of the Earth (Navalgund, Jayaraman & Roy, 2007). RS takes advantage of the electromagnetic spectrum and is broadly categorized into passive sensing (measuring the radiation emitted or reflected from the earth from natural sources) and active sensing sensors (which produce their own electromagnetic radiation and then derive measurements based on how that radiation reflects off the earth). The presence of atmospheric transmission windows (regions of the electromagnetic spectrum that can pass through the atmosphere relatively unimpeded) is what makes remote sensing possible. Readings are made by measuring radiation reaching the sensor which then

analyses it and drawing conclusions based on our knowledge of how radiation scatters off different materials, and on our knowledge of atmospheric interference. This data are then reanalysed and fed into ocean current models as initial conditions and forcing data.

1.4 Global current modelling approaches

Global ocean circulation is driven by energy input, the laws of density, and the physical laws of conservation of mass, momentum, and energy. Since the driving factors of ocean circulation are fundamental physics, ocean circulation can be modelled with equations.

The Geophysical Fluid Dynamics Laboratory developed the first significant ocean model in the 1960s to be used in conjunction with atmospheric models to study climate (Semtner, 1995). There are several spatial and temporal considerations required with ocean modelling based on the computational power available to the model. Improved mathematics and computational power allow for spherical coordinated equations and specified global geometry (Semtner, 1995). Comparison of early ocean models to drifter data showed that mesoscale eddies account for the bulk of kinetic energy in the ocean, and move in a way that was not adequately described by the macroscale ocean models (Lee Dantzler, 1976). The need to include mesoscale events led to further refinements and reengineering of ocean circulation models, pre-filtering equations and limiting some types of data input (Holland, 1978). The need to include mesoscale and sub-mesoscale events also led to the inclusion of complexities like surface boundary interfaces, sea-ice interactions, and regional bathymetry (Semtner, 1995; Lellouche et al., 2022). Today, most models of ocean dynamics (including circulation) run on what

are known as the primitive equations, nonlinear partial differential equations on the laws of conservation and thermodynamics (Häfner, Nuterman & Jochum, 2021).

1.5 The focus of this study

The Operation Mercator global ocean physical analysis and forecasting product (Mercator data product) is hosted by Copernicus Marine Data Store. The Mercator data product provides three-dimensional ocean current data for the global ocean every six hours on a 1/12-degree grid, based on the governing equations of fluid flow and the equations of state. An overview of how the model works and the data it assimilates is provided in the 2.2.1 Modelled data section of the methods. Even though it is a new data product (launched November 2022) it has already been used extensively as a data source for a wide range of works. This includes mapping industrial activity at sea (Paolo et al., 2024), pollution and oil spill monitoring and modelling (Abdallah & Chantsev, 2022; Njutapvoui et al., 2023; Zhang et al., 2023), circulation and frontal dynamics (Calvino, Dabrowski & Dias, 2022; Pak et al., 2023; Qiu et al., 2023; Wang, et al., 2023), upwelling and productivity predictions (Chávez-Castrillón et al., 2023; Lorente et al., 2023), larval dispersal studies (Bertolini & Pastres, 2023), turtle tracking (Barbour et al., 2023), fisheries forecasting (Armas, Arancibia & Neira, 2022), and fuel optimization (Armas, Arancibia & Neira, 2022; Nguyen et al., 2023).

Model products like the Mercator data product are only as useful as they are trustworthy. For this reason, modellers and space agencies have strategies to validate the performance of satellite derived, reanalysis, and modelled datasets. Validation is the process of independently evaluating the accuracy of product outputs and quantifying their uncertainties through comparison with reference data (Justice et al.,

2000). Validation intends to ensure that the data are suitable for the purposes of the end user and that the data represent the 'true' reading (Loew et al., 2017). This study will validate the ocean currents simulated by the Mercator data product with ADCP data for use in local applications of the south-east Atlantic, within the southern Benguela Upwelling System.

ADCPs are a universally recognized *in-situ* device to measure water movement (e.g. currents, turbulence, tides) and are widely used in validation works (Williams, Heron & Anderson, 2008; Baxley, 2013). Rozman et al. (2011) validated both satellite-derived and modelled sea-ice drift in the Laptev Sea by comparing modelled output data to *in situ* measurements taken with an ADCP. de Pablo et al. (2019) validated a hydrodynamic model against ADCP measurements, CTD casts (conductivity, temperature, depth), and tide gauge data in the Tagus coastal area. Togneri et al., (2017) validated the use of a Regional Ocean Modelling System (ROMS) for quantifying turbulence in tidal energy using measurements taken by an ADCP using correlation and root-mean-square-error (RMSE) metrics. Dalsøren et al., (2020) also validated ROMS products using ADCP and CTD data in a fjord in Norway. Sudhan Saravana Prabahar et al., (2022) used ADCP data to validate an actuator line model of the impact of tidal flow on a power plant. Kristensen & Gusdal (2021) used ADCP data to validate both a current model (called NorKyst800), and the use of ships as validation tools for current models. Above is only a small selection of current model validation studies that utilise ADCP data as *in situ* data sources. In all cases, modeled and measured data are matched spatially and temporally, to provide a more direct comparison.

Due to the wide use of ADCP data to validate current models a similar approach was used in this study. An ADCP deployed in the southern Benguela Upwelling System (Figure 3) was programmed to record ten months of current data. This was compared to the Mercator data product outputs in the region for the same time period. This study intended to assess the ability of the Mercator data product to:

1. Capture the overall trends (magnitude and direction) of the measured currents
2. Capture the variability of the measured currents
3. Capture the seasonality of the measured currents.

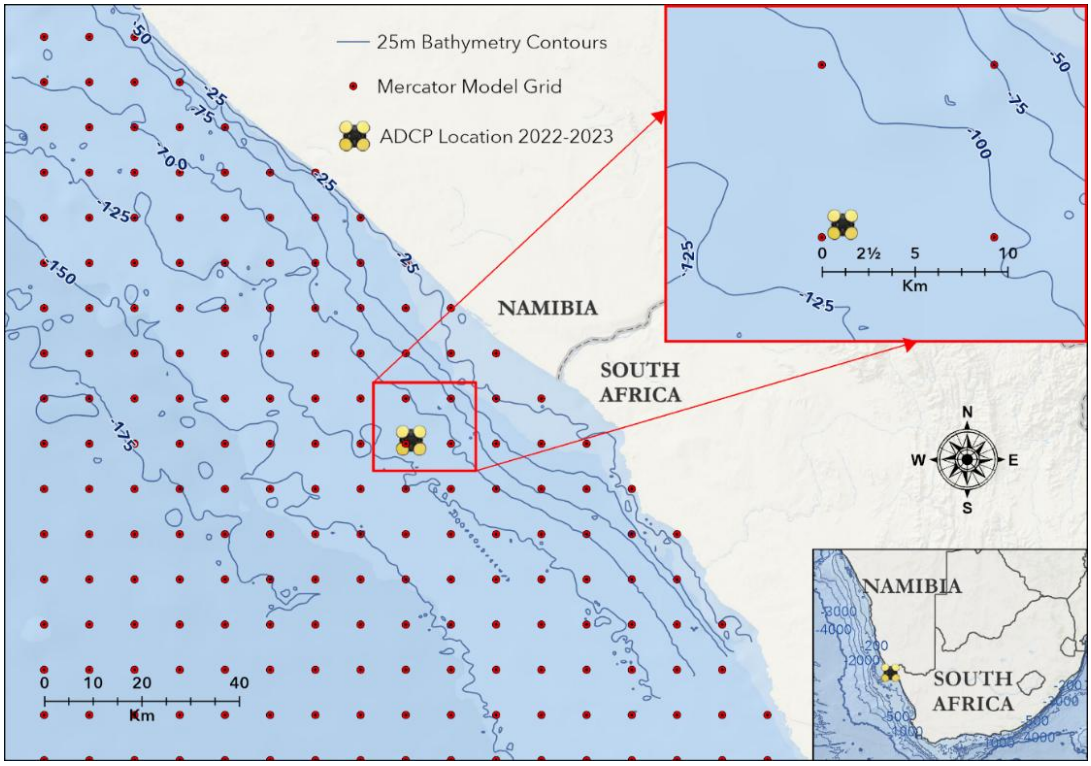

Figure 3. Grid of locations of the Mercator data product and deployment location of the ADCP.

2 Methods

2.1 Approach

This study compared modelled data sourced from the Marine Copernicus Operational Mercator global sea physical analysis and forecasting product against in situ data captured by an Acoustic Doppler Current Profiler (ADCP) deployed for a cumulative period of ten months at a site in the south-eastern Atlantic Ocean, near the border of South Africa and Namibia. Data were spatially and temporally matched, filtered, and analysed. The analysis covered simple summary statistics (mean, max, standard deviation), correlation, root-mean-square-error, bias, and percentage occurrence. Statistics were chosen to be comparable to previous studies validating ocean current products in other regions (e.g., (Johnson et al., 2007; Blockley, Martin & Hyder, 2012; Sikhakolli et al., 2013; Lorente, Piedracoba & Fanjul, 2015; Chao et al., 2018)).

2.2 Data

2.2.1 Modelled data

The Marine Copernicus Operational Mercator global sea physical analysis and forecasting product (the Mercator data product) is a global ocean forecasting model that outputs six-hourly, daily, and monthly means of sea level height, salinity, temperature, horizontal and vertical currents, and variables around sea ice. It is updated daily at noon UTC and has a horizontal resolution of 1/12 degree across 50 vertical levels. We made use of the six hourly current data at 20 depths available in the Mercator data product for this study. It is available for download from the Copernicus Marine Data Store (https://doi.org/10.48670/moi-00016), with a time series starting in June 2020 at the time it was made publicly available. The Mercator

data product is derived from a high-resolution system called GLOBAL_ANALYSIS_FORECAST_001_024 version 4 (GLO12v4).

The GLO12v4 system is configured to run on version 3.6 of the Nucleus for European Modelling of the Ocean (NEMO). The following paragraphs are a description of NEMO and how it functions, summarised from Madec & NEMO team (2016), with the parameterization used by The GLO12v4 system detailed in Lellouche et al. (2022).

NEMO was developed from the OPA model, a regional and global equation model for ocean circulation (Madec et al., 1998). The basics of the model are built on the Navier-Stokes equations - linking temperature and salinity as active tracers to the fluid velocity of the ocean waters, which are the momentum equations in the vector invariant form. In GLO12v4 these advection traces are computed using a total variance diminishing advection scheme, which handles flux forms (Madec et al., 1998). The basic equations follow a vertical curvilinear coordinate system due to the vertical variability of the ocean. Aspects such as moving surface currents, variable bottom depth, and thermohaline stratification require this generalized coordinate system (Kasahara, 1974). Sub-grid scale physics (like turbulence) are parameterized rather than being explicitly solved for, GLO12v4 system uses a ‘partial cells’ parameterization.

A time stepping strategy is the order a model solves its equations, as some outputs feed into other equations. NEMO's time stepping environment is structured in such a way to allow terms to operate ‘before’, ‘now’, or ‘after’. Non-diffusive aspects of the model (momentum, pressure gradients, Coriolis terms, etc.) employ a leapfrog scheme that is time centred on the ‘now’ time (Mesinger & Arakawa, 1976). Lateral

diffusive or damping processes (friction, heat flux, etc.) use a forward time differencing scheme. Vertical diffusion uses a forward time differencing scheme with a time splitting technique, or a backward time differencing scheme (Madec & NEMO team, 2016).

As well as being arranged in time, variables also need to be arranged in space. This is done using the Arakawa C grid, which consists of cells centred on scalar points with vector points in the centre of each face of the cell (Mesinger & Arakawa, 1976). The grid (called the ocean mesh) also defines the mathematical locations of the relative and planetary vorticity and the barotropic stream function. The vertical ocean mesh is determined by the regional bathymetry, the number of levels in the model, the analytical transformation, and the masking system. The horizontal grid domain, vertical grid domain, and metre bathymetry are all configurable within NEMO by the user. The GLO12v4 system uses the tripolar ORCA12 grid type which has a horizontal resolution of 9 km at the equator, 7 km at the mid-latitudes, and 2 km in the Ross and Weddell seas (Lellouche et al., 2022). Glo12v4 uses a combination of two bathymetric databases, ETOPO1 for regions deeper than 300 m and GEBCO8 for regions shallower than 200 m. The vertical bins used depend on the bottom topography data available for an area, and whether a given layer is a linear free surface or not (Madec & NEMO team, 2016). Linear free surfaces are at a z-coordinate level that is fixed in time, while non-linear free surfaces use a rescaled formula for the z-coordinate with a level position that varies in time as a function of sea surface height. The Mercator data product outputs 50 (non-linearly distributed) vertical bins between the surface and a maximum depth of 5 000 m (Lellouche et al., 2022). The model does not reproduce tides or vertical velocity.

Active traces in oceanic modelling are variables (or substances) included in the model to simulate the transport, dispersion, and behaviour of a material or property in the ocean (Treguier, 2006). In the NEMO model, there are two active tracers - potential temperature and salinity. They are modelled using advection, lateral and vertical diffusion, and external forcings (e.g. surface boundary conditions, internal damping, and penetrative solar radiation) (Madec & NEMO team, 2016). Each of these components has its own sets of equations, rules and orders for when they are executed for each time step. In GLO12v4 a Laplacian lateral isopycnal diffusion operator is applied (Lellouche et al., 2022). Equations of state (EOS) provide the link between active tracers and fluid dynamics (Fofonoff & Millard, 1983). The EOS are broken into three parts; the equation of seawater (empirical nonlinear thermodynamic relationship linking seawater density to temperature, salinity, and pressure), Brunt-Väisälä Frequency (ocean stability for ocean stratification), and the freezing point of seawater (also a function of salinity and pressure) (Madec & NEMO team, 2016).

Data fed into GLO12v4 come from multiple sources using a reduced-order Kalman filter method. Data are assimilated from L3 sea level anomaly, L3 sea surface temperature, L4 sea ice concentration, *in situ* temperature, and *in situ* salinity. Data processing is done to adapt forecast errors, state anomalies, and bias correction. Data are sourced from subbranches of the Copernicus Marine program.

2.2.2 ADCP data

In situ reference data for this study were obtained from an upwards-looking moored Nortek Signature250 ADCP (Sig250). ADCPs employ acoustic transducers that send pings into the water column and ‘listen’ to the backscatter off particles in the water

column. They operate with at least three sensor heads and use triangulation and the Doppler shift to calculate the movement of the particles in the water and derive water movement from these data. The device was deployed at a depth of 123 m in the nearshore southern Benguela upwelling system (Figure 3, Lat: -28.763204 Lon: 16.163626) on the 24th November 2022 and retrieved on the 23rd May 2023, then redeployed on the 4th August 2023 and retrieved on 26th November 2023. The approach this study took was influenced by high vessel traffic in the area which necessitated an upwards-facing ADCP configuration. The exact deployment location was dictated by other projects also requiring the data collected. The Nortek Sig250 has a profiling range of 200 m with a maximum sampling rate of 3 Hz with a transducer acoustic frequency of 250 Hz from four beams. The Nortek Sig250 was configured to measure for a two-minute window every thirty minutes in 2 m vertical bins. This outputs vector component current data for a single depth at 2 m intervals. The ADCP performs a correlation function in each cell for every ping, for each beam to measure the similarity between observations (Nortek Group, 2017). Data below a threshold is replaced with interpolated data. The final ADCP data comes with an indication of 'Percent good' (Table 1), the percentage of data points above 50% correlation for each depth over the time series (Nortek Group, 2022). Depths four and six metres are the only ones in the series with a 'percentage good' score under 80 (41% and 56% respectively). Echo intensity measured by the ADCP decreases with distance from the sensor heads due to beam spreading and sound attenuation. Subsequently, upwards-looking ADCPs cannot measure ocean currents close to the surface accurately (Gordon, 1996). For this reason, the upper 12 m were included in the summary analysis, but not the percentage contribution aspect (detailed below).

2.2.3 Data analysis

All data analysis was carried out in R studio, R version 4.1.0 using packages tidyr, ncdf4, lubridate, zoo, and dplyr (pseudo code available in Appendix 3). The Mercator data product currents are available at 6-hourly intervals, so it was necessary to temporally aggregate the higher resolution ADCP data through the water column.

To match on a spatial scale, the Mercator data product were cropped to the closest grid cell (Figure 3, Lat: -28.750 Lon: 16.167) which is 1.4 km away from where the ADCP was deployed. Depths measured by the ADCP without a corresponding depth simulated by the Mercator data product were excluded, leaving 20 depths for analysis (Table 1). To match the data on a temporal scale, the ADCP data was reformulated as a rolling average over the preceding six hours. A rolling mean allows for the averaging of a number of data points over a set time window that shifts with each time step calculated. The data were analysed in the zonal (east-west) and meridional (north-south) form (U and V vectors) to negate the need for circular statistics that cardinal direction would require. All observations with zonal or meridional values greater than 0.75 m/s were removed as this is the fastest speed typically recorded in the Benguela Upwelling System and anything greater than this is likely a sensor error (Veitch et al., 2018).

Table 1. Depths for which the Mercator data product current data is available and corresponding depth bin of the ADCP. Number of readings per depth that are available from both the Mercator data product and the ADCP, and the percentage good value given by the ADCP.

Mercator data product depth (m)	ADCP depth (m)	Number of readings	% good readings
2.6	2	1154	91.59
3.8	4	487	41.10
6.4	6	585	54.51
7.9	8	1138	89.39
9.6	10	1070	86.14
11.4	12	959	83.72
13.5	14	1137	96.33
15.8	16	1158	97.36
18.5	18	1170	97.93
21.6	22	1171	98.19
25.2	26	1173	98.13
29.4	30	1173	97.99
34.4	34	1174	97.84
40.3	40	1170	97.51
47.4	48	1170	97.26
55.8	56	1161	96.84
65.8	66	1161	96.58
77.9	78	1155	96.42
92.3	92	1160	96.01
109.3	110	1126	93.11

Data were checked for normality using both Q-Q plots and histograms. The ADCP zonal and meridional data and the zonal component of the Mercator data product were not normally distributed (Figure 4). No statistical assessment was done to check for

normality as statistical normality tests lose power when sample sizes are > 900 (Demir, 2022). Given that the data were collected from an upwelling system with strong seasonality, the data were split into seasons for a more in-depth assessment of performance. Seasons were defined as follows: Summer = 1 December to 28 February, Autumn = 1 March to 31 May, Winter = 1 June to 31 August, and Spring = 1 September to 31 November. The following statistics were calculated for both the full data set, and the seasonal components:

1. Summary statistics (Mean, maximum, and standard deviation) were presented for both the Mercator data product and ADCP data at all depths. Mean and standard deviation were calculated using the full data sets in each case. With vector components, the direction was coded into the sign. The maximum metric was taken as the greatest absolute value, and then the direction was added back.
2. Root-mean-square-error (RMSE) was calculated using Equation 1 where '*n*' is the number of available data points. RMSE is a measure of the standard deviation of the residuals; how far the modelled values are from the regression line. Smaller absolute RMSE values indicate better model simulations.

$$RMSE = \sqrt{\frac{\sum_{i=1}^{n}(ADCP_i - Mercator_i)^2}{n}} \qquad \text{Equation 1}$$

3. Correlation measures the strength of the relationship between modelled and measured data. Spearman's Rank Correlation (correlation) was used as a non-parametric correlation metric to assess the strength and direction of association between the two data sets. Correlation was calculated using Equation 2, where '*n*' is the number of points in the dataset, and 'd_i' is the difference in the ranks

of the ADCP and the Mercator data product coordinates. The Spearman's Rank Correlation assumes a value between -1 and 1 which indicates the strength of the relationship. A value of 0 indicates there is no monotonic relationship between the variables, values closer to 1 indicate a strong positive relationship, and -1 a strong inverse relationship.

$$\rho = 1 - \frac{6\sum d_i^2}{n(n^2-1)} \qquad \text{Equation 2}$$

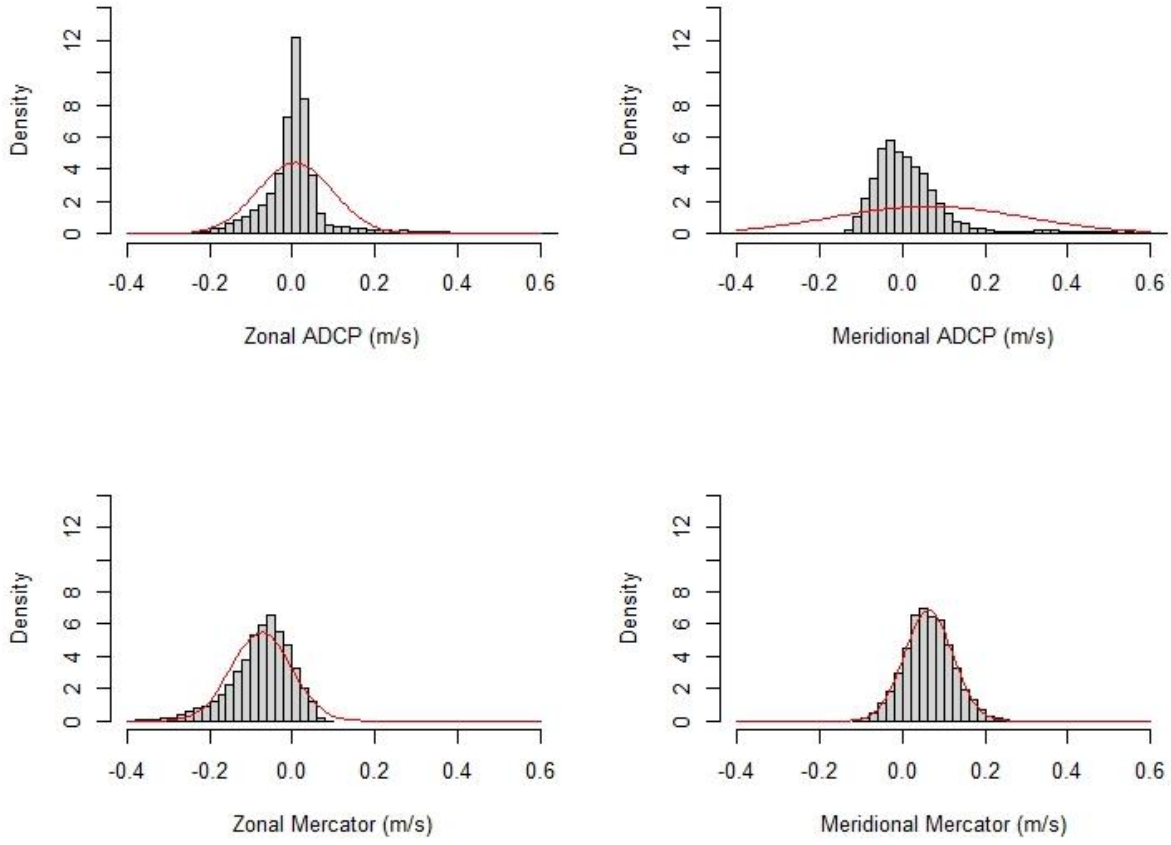

Figure 4. Probability of occurrence of zonal (left) and meridional (right) current vectors (speed and direction) by the ADCP (top) and the Mercator data product (bottom) with a hypothetical 'normal' distribution presented in red.

4. Bias (sometimes called mean error) is the mean difference between modelled and measured data (Equation 3). A negative bias implies the model is consistently simulating smaller values than those measured, while a positive bias implies the model is simulating larger values than those measured.

$$\frac{\sum(ADCP_i - Mercator_i)}{n} \quad \text{Equation 3}$$

Blockley et al., (2012) observed that for velocity fields such as those assessed in this study, bias potentially offers poor information on the difference between the two datasets due to the directional nature of the velocities, particularly in areas with currents travelling in opposite directions.

5. Percentage occurrence. To understand the seasonality of the system and the performance of the Mercator data product within each season, percentage occurrence for U and V components was calculated for three current velocity bands (slow: 0-0.2, moderate: 0.2-0.4, high: 0.4-0.6 m/s). For this section of the analysis, depths shallower than 14 m were excluded, due to the lower reliability of the ADCP data in this zone (indicated by the % good data column of Table 1). Each data point in the series can be identified by its depth, season, direction, and velocity (presented in Figure 5).

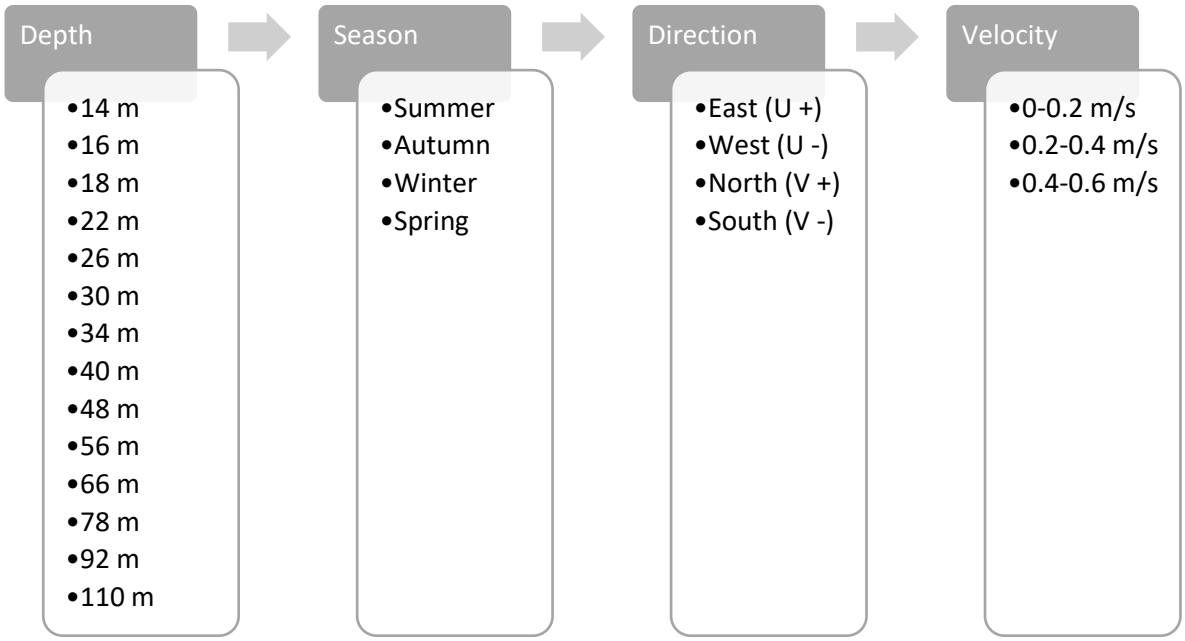

Figure 5. Visual representation of data categories used in the percentage component analysis.

Percentage occurrence was calculated for each depth band in each season as the number of occurrences at a given direction and velocity in that given seasonal depth band over the number of data points in that seasonal depth band. Equation 4 gives the example equation for slow zonal speeds in an easterly direction (U +) in summer at 14 m.

$$\frac{n_{(14\ \mathrm{m}\ summer\ U+0-0.2)}}{n_{(14\ \mathrm{m}\ summer)}} \qquad \text{Equation 4}$$

Percentage occurrence was calculated for both the Mercator data product and ADCP data for all times when data were available for both datasets. Given that there are fourteen depth options, four seasons, four vectors, and three velocity bands for both the ADCP dataset and the Mercator data product, there are 1 344 percentage occurrence data values calculated.

Due to little interseasonal variation, a decision was made to present the full time series rather than a seasonal breakdown in the results section for mean, standard deviation, correlation, RMSE, and bias. A full seasonal breakdown is provided in the Appendix. A seasonal split was presented for the percentage occurrence statistics.

3 Results

Ocean currents measured by the ADCP were compared to the corresponding current simulated by the Mercator data product. Currents were compared separately by seasons, for the zonal and meridional vector components due to the seasonal upwelling nature of the system. In both summer and winter, ADCP and Mercator data product zonal current vectors throughout the water column showed a daily directional oscillation (Figure 6 & Figure 7). Currents in the upper 30 metres followed the same period meridional oscillation, flowing northwest around midnight, west around 06h00, south around 12h00 and southeast around 18h00. This signal was more regular in the summer months, but still present in winter (Figure 6 & Figure 7). The fastest current speeds were found in the top two metres of the water column in March and November (~0.74 m/s), averaging 0.26 m/s (SD = 0.35 m/s) over the full time series (Table 2). Current speeds slowed with increasing depth, with a comparatively large drop in speed at 10 m. The slowest waters were found at 110 m, with the average speed being 0.03 m/s (SD = 0.02 m/s). Current directional variability followed the same trend as speed, dropping with increasing depth.

A more in-depth comparison of the ADCP and the Mercator data product datasets, split into the zonal and then meridional components, is included in the sections that follow.

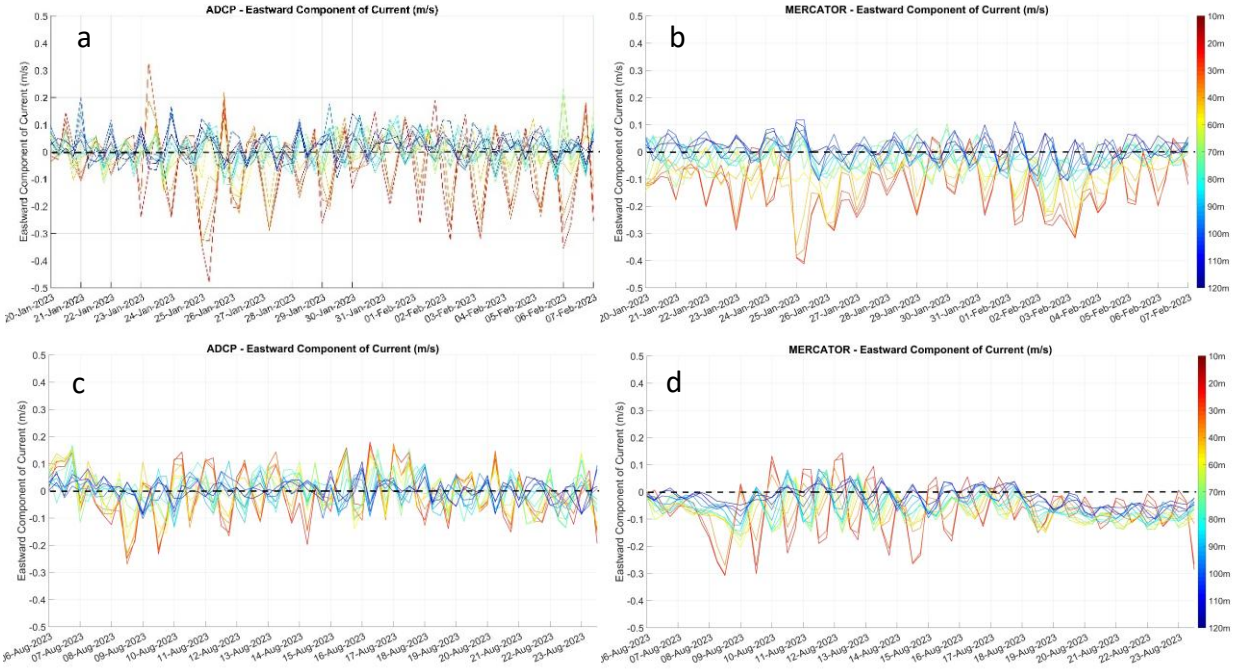

Figure 6. Zonal or West-East Component of Currents (m/s) at selected depth zones (10 – 110 m Table 1) for (a) Summer ADCP, (b) Summer Mercator, (c) Winter ADCP, (d) Winter Mercator where ADCP observations were time averaged for 17 days in summer (Jan-Feb) and winter (Aug).

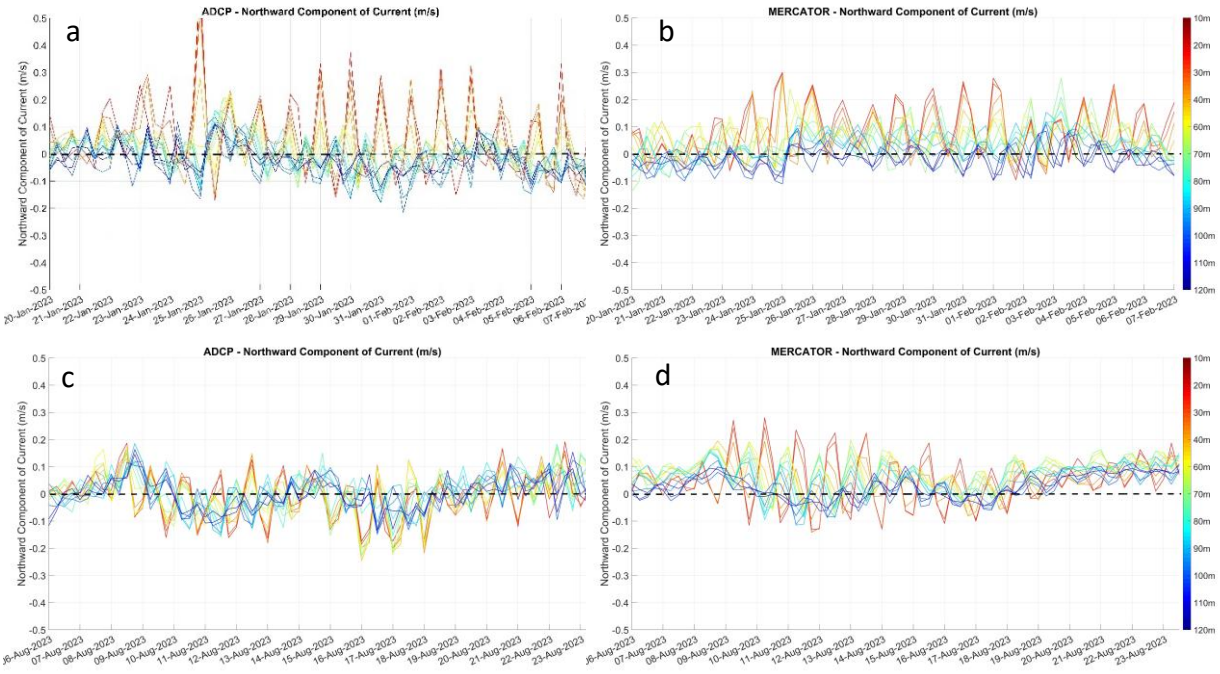

Figure 7. Meridional or North-South Component of Currents (m/s) at selected depth zones (10 – 110 m Table 1) for (a) Summer ADCP, (b) Summer Mercator, (c) Winter ADCP, (d) Winter Mercator where ADCP observations were time averaged for 17 days in summer (Jan-Feb) and winter (Aug).

3.1 Zonal component

To understand the degree of variance between the ADCP measurements and simulation outputs from the Mercator data product at each depth, the mean zonal vector at each depth and standard deviation (in parentheses) is presented in Table 2. These statistics were calculated using the full time series, as there was little variation between seasons. Seasonal summary statistics are provided in Appendix 1. Mean zonal vector values indicate the net direction of water movement at each depth, with negative values indicating westward (offshore) and positive values indicating eastward (onshore) flow. The ADCP values indicated eastward movement at 2-10 m depth, westward at 12-26 m (Figure 8-a), and then eastward movement at 30-110 m depth (Figure 8, Table 2), whereas the Mercator data product represented a net westward

movement at all depths over the time series. Both data sources indicated that the highest variability (based on the standard deviation) was found above 10 m while steadily decreasing variability with depth. Below a depth of 8 m, the variability of the ADCP and the Mercator data product are similar (seen in the comparable period and amplitude of the oscillation presented in Figure 8).

Table 2. Statistical comparison between *in situ* (ADCP) and modelled (Mercator data product) zonal currents (m/s) for all depth bins. Mean (± standard deviation) and greatest current vector (Max) for the ADCP and the Mercator data product data, root-mean-square-error (RMSE), Spearman's rank correlation (ρ), and bias comparisons between *in situ* and modelled data.

Depth (m)	Mean (± SD) ADCP	Mean (± SD) Mercator data product	Max ADCP	Max Mercator data product	RMSE	ρ	bias
2	0.138 (± 0.317)	-0.105 (± 0.124)	-0.735	-0.416	0.411	0.09	0.243
4	0.08 (± 0.347)	-0.126 (± 0.141)	0.742	-0.496	0.387	0.36	0.206
6	0.104 (± 0.298)	-0.129 (± 0.137)	0.733	-0.492	0.364	0.37	0.234
8	0.025 (± 0.152)	-0.133 (± 0.125)	-0.568	-0.49	0.221	0.39	0.159
10	0.002 (± 0.091)	-0.13 (± 0.125)	-0.45	-0.488	0.177	0.41	0.133
12	-0.034 (± 0.141)	-0.124 (± 0.124)	-0.531	-0.486	0.172	0.39	0.09
14	-0.051 (± 0.12)	-0.117 (± 0.12)	-0.501	-0.484	0.147	0.37	0.065
16	-0.04 (± 0.11)	-0.113 (± 0.114)	-0.493	-0.482	0.145	0.34	0.072
18	-0.03 (± 0.101)	-0.101 (± 0.102)	-0.473	-0.478	0.138	0.28	0.07
22	-0.014 (± 0.089)	-0.086 (± 0.088)	-0.427	-0.468	0.131	0.19	0.071
26	-0.006 (± 0.078)	-0.073 (± 0.076)	-0.357	-0.422	0.115	0.23	0.067
30	0 (± 0.068)	-0.062 (± 0.069)	-0.329	-0.336	0.103	0.26	0.062
34	0.003 (± 0.062)	-0.053 (± 0.065)	-0.313	-0.299	0.093	0.29	0.057
40	0.007 (± 0.055)	-0.045 (± 0.06)	-0.253	-0.257	0.085	0.31	0.053
48	0.011 (± 0.051)	-0.043 (± 0.059)	0.179	-0.239	0.082	0.32	0.054

Depth (m)	Mean (± SD) ADCP	Mean (± SD) Mercator data product	Max ADCP	Max Mercator data product	RMSE	ρ	bias
56	0.012 (± 0.05)	-0.033 (± 0.06)	0.18	-0.239	0.081	0.27	0.046
66	0.013 (± 0.049)	-0.022 (± 0.057)	0.199	-0.211	0.074	0.24	0.035
78	0.014 (± 0.044)	-0.015 (± 0.059)	0.221	-0.192	0.07	0.24	0.03
92	0.015 (± 0.038)	-0.006 (± 0.055)	0.169	-0.186	0.059	0.31	0.022
110	0.014 (± 0.031)	-0.003 (± 0.039)	-0.16	0.111	0.044	0.34	0.018

Root-mean-square-error (RMSE) is a measure of deviation between the ADCP and modelled data, with smaller absolute values indicating lower deviation. RMSE decreased from 0.44 at 2 m to 0.04 at 110 m, with very little variation below 26 m (Table 2). Bias is the mean of the difference between observational and simulated data. Lower bias indicates lower overall differences but needs to be considered with the scale of measurements in mind. In this case, the bias is comparable to (or less than) the standard deviation measured by the ADCP at all depths except 10 m (Table 2). This means that the currents represented by the Mercator data product are (on average) within the natural variability of the system. Spearman's rank correlation (correlation) indicates how well two variables can be described using a monotonic function (a function where the relationship between the two variables is always increasing or decreasing; in this case, higher zonal ADCP values should always be associated with higher zonal Mercator data product values). Higher values indicate a stronger correlation. Zonal correlation was strongest at 10 m depth, (measuring 0.41) and weakest at 2 m depth (measuring 0.09) (Table 2), however, the data were less correlated around 22 m but were almost all above 0.25 (except at 2 m, 66 m and 78 m).

Comparative metrics on zonal vectors in the upper 10 m did not perform well. This is likely due to the high variability in this region, as well as to the poor quality of measured data from the ADCP in this zone due to beam spreading and sound attenuation resulting in decreased echo intensity (Gordon, 1996). Adding to this are the limitations of the Mercator data product which does not yet include the effects of waves or tides (Lellouche et al., 2022). As a result, the next part of this section breaks down seasonal trends recorded by the ADCP and simulated by the Mercator data product at depths below 14 m.

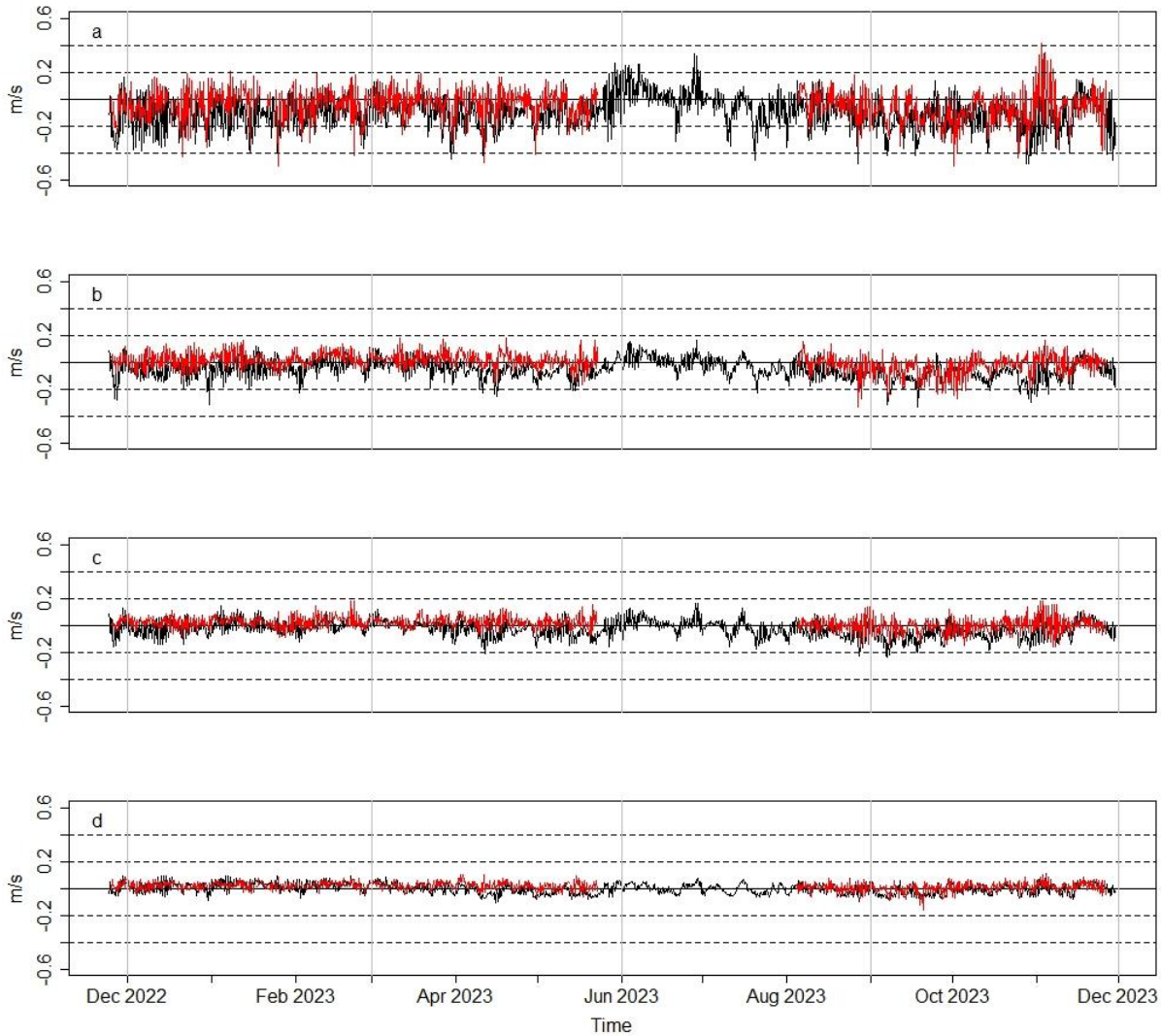

Figure 8. Zonal time series data from the ADCP (red) and the Mercator data product (black) at depths of (a) 14 m, (b) 30 m, (c) 56 m, and (d) 110 m. A six-hourly running

Figure 8. continued mean is applied to the available ADCP data. No ADCP data is available for the June-July period. Vertical grey lines denote seasonal splits (starting with summer to the right of Dec 2022), and horizontal dotted lines show breaks between slow (0-0.2 m/s), moderate (0.2-0.4 m/s), and high (0.4-0.6 m/s) current velocities. Negative values indicate a westerly (onshore) direction, positive values are easterly (offshore). These depths were selected for their spread through the water column and for their clarity on the general trends.

Table 3 presents the proportions of time that water at a given depth (14-110 m) was moving in an eastward or westward direction during each season, presented in the velocity category for each (slow: <0.2 m/s, moderate: 0.2-0.4 m/s, and high: 0.4-0.6 m/s) as measured by the ADCP or simulated in the Mercator data product.

In summer, measured zonal currents were moving at slow speeds >80% of the time. Between 14 and 22 m these slow speeds were primarily westward, wheras below 22 m they were predominantly eastward (49-74% occurrence). Moderate current speeds were typically found in depths shallower than 34 m, with the highest instances of moderate water movement (17%) measured at 14 m. Moderate currents followed the same directional behaviour as slow currents. High currents were mostly found at 18 m and above, but at very low frequencies, and were consistently moving west. The Mercator data product matched the predominant direction of slow currents between 14 and 18 m. Between 22 and 56 m, the Mercator data product represented a predominant westward slow current, which is inconsistent with the measured data. Below 66 m depth, slow currents simulated in the Mercator data product followed the same direction and were of a similar magnitude to the measured data (≤ 8%

occurrence). The Mercator data product overrepresented the frequency of moderate westward currents by more than 50% (seen visually in Figure 8-b for 30 m depth, but true for 14-30 m) and did not represent any of the measured eastward currents.

Slow zonal velocities were measured in >90% of the autumn period, with most of the remaining current occurrences being moderate. Similar to in summer, water movement in the upper 22 m was mostly westward, with waters below that typically moving eastwards. Most moderate currents were found at 14-18 m moving westward (15%), though moderate eastward currents were also measured. High velocity currents were occasionally recorded moving west (0.6% of the time between 14 and 18 m). Above 30 m in autumn, the Mercator data product underrepresented slow currents by as much as 10%. It simulated the bulk flow direction to be westerly at every depth (seen in Figure 8 where the black line is mostly found below the 0 (negative) compared to the measured). Moderate currents in a westerly direction were overrepresented and those in an easterly direction were missed entirely. However, the Mercator data product did capture the direction and general frequency of the high westerly currents in the upper ocean (Figure 8-a).

In winter, there was a near equal split between westward and eastward slow currents. At depths of 16 m, 26-40 m, and 56-110 m the predominant direction was westward; however in all depths above 78 m there was a less than 5% difference between the frequency of westward and eastward currents. More than 90% of the time, the currents were slow. The upper 20 m had moderate currents moving westward approximately 10% of the time, with lower frequencies of moderate westward currents recorded in the top 40 m. There were no records of high currents during winter in the ADCP data.

August was the only true winter month for which comparisons were available with the Mercator data product (Figure 8). The Mercator data product once again contained more moderate currents and fewer slow currents at 14 and 16 m than were measured in the ADCP data. The Mercator data product simulated slow westward currents at all depths, overrepresenting the frequency of this direction by as much as 40% below 18 m. In the upper 20 m it also simulated high westerly currents not measured in the ADCP data.

Table 3. Percentage occurrence of current velocity and direction for zonal ADCP (Mercator data product) currents. Current velocity bands (slow: 0-0.2, moderate: 0.2-0.4, high: 0.4-0.6 m/s) in the eastward (E (U+)) and westward (W (U-)) direction presented at 14 depths for Summer (1 Dec to 28 Feb), Autumn (1 Mar to 31 May), Winter (1 Jun to 31 Aug), and Spring (1 Sep to 31 Nov). Values in bold indicate the bulk direction for each current velocity band at each depth.

	0-0.2 m/s		**0.2-0.4 m/s**		**0.4-0.6 m/s**	
Depth	**E (U+)**	**W (U-)**	**E (U+)**	**W (U-)**	**E (U+)**	**W (U-)**
Summer						
14	37.5 (21.87)	**44.03 (52.55)**	1.98 (0)	**15.34 (25.28)**	0 (0)	**0.56 (0.28)**
16	40.2 (19.55)	**48.32 (56.7)**	2.51 (0)	**8.37 (23.46)**	**0.27** (0)	**0.27 (0.27)**
18	42 (17.82)	**50.97 (63.78)**	1.11 (0)	**5.29 (18.38)**	0 (0)	**0.27** (0)
22	**49.1** (20)	47.22 **(70)**	**1.38** (0)	**1.38 (10)**	0 (0)	0 (0)
26	**55.2** (20.55)	42.5 **(75.55)**	**0.83** (0)	0.55 **(3.88)**	0 (0)	0 (0)
30	**59.4** (26.38)	39.16 **(72.77)**	**0.27** (0)	0.55 **(0.83)**	0 (0)	0 (0)
34	**59.7** (32.77)	39.16 **(67.22)**	**0.27** (0)	**0.27** (0)	0 (0)	0 (0)
40	**63.8** (39.44)	35.83 **(60.55)**	0 (0)	0 (0)	0 (0)	0 (0)
48	**66.6** (38.61)	32.22 **(61.38)**	0 (0)	0 (0)	0 (0)	0 (0)
56	**69** (42.06)	30.64 **(57.93)**	0 (0)	0 (0)	0 (0)	0 (0)
66	**65.6 (53.35)**	33.79 (46.64)	0 (0)	0 (0)	0 (0)	0 (0)

Depth	0-0.2 m/s		0.2-0.4 m/s		0.4-0.6 m/s	
	E (U+)	W (U-)	E (U+)	W (U-)	E (U+)	W (U-)
78	**68.3 (60)**	31.11 (40)	**0.27** (0)	0 (0)	0 (0)	0 (0)
92	**74.3 (71.3)**	24.51 (28.69)	0 (0)	0 (0)	0 (0)	0 (0)
110	**72.4 (74.93)**	26.74 (25.06)	0 (0)	0 (0)	0 (0)	0 (0)
Autumn						
14	37.83 (14.41)	**51.95 (67.56)**	1.8 (0)	**7.8 (17.11)**	0 (0)	**0.6 (0.9)**
16	39.6 (14.71)	**51.95 (69.96)**	1.8 (0)	**5.7 (14.41)**	0 (0)	**0.6 (0.9)**
18	41.3 (13.47)	**51.49 (74.85)**	1.19 (0)	**4.79 (11.37)**	0 (0)	**0.59 (0.29)**
22	**48.3** (16.51)	47.14 **(75.97)**	1.2 (0)	**2.7 (7.5)**	0 (0)	0 (0)
26	**52.9** (18.26)	46.1 **(77.84)**	**0.89** (0)	0 **(3.89)**	0 (0)	0 (0)
30	**57.4** (18.86)	41.01 **(79.34)**	**0.89** (0)	0.29 (**1.79)**	0 (0)	0 (0)
34	**58** (19.46)	41.01 **(79.94)**	0 (0)	0 **(0.59)**	0 (0)	0 (0)
40	**63.7** (21.25)	35.62 **(78.14)**	0 (0)	**0.29 (0.59)**	0 (0)	0 (0)
48	**64.9** (23.95)	34.13 **(75.74)**	0 (0)	0 **(0.29)**	0 (0)	0 (0)
56	**67.3** (29.94)	32.63 **(69.76)**	0 (0)	0 **(0.29)**	0 (0)	0 (0)
66	**66.1** (32.32)	32.93 **(67.67)**	0 (0)	0 (0)	0 (0)	0 (0)
78	**66.9** (30.63)	32.73 **(69.36)**	0 (0)	0 (0)	0 (0)	0 (0)
92	**69.3** (33.63)	30.33 **(66.36)**	0 (0)	0 (0)	0 (0)	0 (0)
110	**67.3** (32.63)	30.83 **(67.36)**	0 (0)	0 (0)	0 (0)	0 (0)
Winter						
14	44.03 (22.93)	**45.87 (62.38)**	0.91 (0)	**9.17 (13.76)**	0 (0)	0 **(0.91)**
16	**46.7** (19.26)	44.03 **(66.97)**	0.91 (0)	**8.25 (12.84)**	0 (0)	0 **(0.91)**
18	42.2 (11)	**48.62 (82.56)**	0.91 (0)	**8.25 (5.5)**	0 (0)	0 **(0.91)**
22	45.8 (6.42)	**46.78 (89.9)**	0 (0)	**7.33 (2.75)**	0 (0)	0 **(0.91)**
26	**47.7** (11.92)	45.87 **(85.32)**	0 (0)	**5.5 (2.75)**	0 (0)	0 (0)
30	**49.5** (9.17)	46.78 **(90.82)**	0 (0)	**3.66** (0)	0 (0)	0 (0)
34	**50.4** (11)	45.87 **(88.99)**	0 (0)	**3.66** (0)	0 (0)	0 (0)
40	**49.5** (12.84)	48.62 **(87.15)**	0 (0)	**1.83** (0)	0 (0)	0 (0)
48	46.7 (7.33)	**53.21 (91.74)**	0 (0)	0 **(0.91)**	0 (0)	0 (0)
56	**50.4** (18.34)	49.54 **(80.73)**	0 (0)	0 **(0.91)**	0 (0)	0 (0)
66	**51.3** (22.01)	47.7 **(77.98)**	0 (0)	0 (0)	0 (0)	0 (0)

Depth	0-0.2 m/s		0.2-0.4 m/s		0.4-0.6 m/s	
	E (U+)	W (U-)	E (U+)	W (U-)	E (U+)	W (U-)
78	**56.8** (24.77)	43.11 **(75.22)**	0 (0)	0 (0)	0 (0)	0 (0)
92	**59.6** (27.52)	40.36 **(72.47)**	0 (0)	0 (0)	0 (0)	0 (0)
110	**54.1** (36.69)	45.87 **(63.3)**	0 (0)	0 (0)	0 (0)	0 (0)
Spring						
14	22.64 (14.82)	**54.44 (50.67)**	1.88 (0)	**18.86 (31.8)**	**0.53** (0)	**0.53** (0)
16	26 (15.05)	**52.95 (53.76)**	2.41 (0)	**17.2 (28.76)**	**0.26** (0)	**0.26** (0)
18	27.1 (13.17)	**55.64 (64.24)**	2.15 (0)	**13.97 (21.23)**	0 (0)	0 (0)
22	32.2 (13.7)	**54.83 (72.31)**	1.61 (0)	**11.02 (13.44)**	0 (0)	0 (0)
26	34.4 (12.09)	**56.98 (78.22)**	0.53 (0)	**8.06 (9.4)**	0 (0)	0 (0)
30	41.6 (13.17)	**53.22 (80.1)**	0 (0)	**5.1 (6.72)**	0 (0)	0 (0)
34	41.9 (11.55)	**53.49 (85.48)**	0.26 (0)	**4.3 (2.95)**	0 (0)	0 (0)
40	42.4 (12.9)	**55.1 (84.94)**	0.26 (0)	**1.88 (2.15)**	0 (0)	0 (0)
48	44.8 (15.05)	**54.03 (83.33)**	**0.53** (0)	0.26 **(1.61)**	0 (0)	0 (0)
56	47 (19.08)	**52.15 (79.56)**	**0.53** (0)	0 **(1.34)**	0 (0)	0 (0)
66	48.3 (24.73)	**50.53 (74.46)**	**0.8** (0)	0 **(0.8)**	0 (0)	0 (0)
78	**51** (27.95)	47.84 **(72.04)**	**0.53** (0)	0 (0)	0 (0)	0 (0)
92	**58** (38.97)	41.66 **(61.02)**	0 (0)	0 (0)	0 (0)	0 (0)
110	**59.4** (37.9)	40.59 **(62.09)**	0 (0)	0 (0)	0 (0)	0 (0)

Spring exhibited the highest incidence of high zonal vectors, present at 14 and 16 m in the ADCP data, with equal amounts of west and east movement. Spring contained the highest proportion of moderate currents (twice as frequent as any other season) all the way down to a depth of 78 m. Moderate currents were moving westward most of the time, though all moderate currents deeper than 48 m were flowing eastwards. Slow currents were primarily westward above 66 m and primarily eastwards below that. The Mercator data product did not represent any high spring currents, over-simulated moderate westward currents by as much as 50% and did not represent any of the moderate eastward currents measured in the ADCP data (Figure 8-a&b).

Furthermore, the Mercator data product underrepresented slow currents in either direction in the top 20 m and overrepresented the westward proportion of slow currents at depths greater than 18 m.

In summary, deviation (RMSE) between measured and predicted currents decreased with depth. The bias of the ADCP data and the Mercator data product was lower than the natural variability measured by the ADCP. The top 10 m had highly variable correlation, with little variability of correlation metrics below 22 m. Autumn and winter had slow currents >90% of the time, with high currents in the top 18 m, moderate currents down to 40 m in winter, and 18 m in autumn. Summer had slow currents 80% of the time. Spring had the lowest instance of slow currents (>40% of the time) and had moderate currents down to a depth of 78 m. In all seasons, the Mercator data product simulated westward moving currents at much higher frequencies than they were measured by the ADCP, often missing eastward movement all together. The Mercator data product also overrepresented high currents in winter and autumn and underrepresented them in spring. The Mercator data product represented the magnitude of the measured zonal data better than it represented the direction.

3.2 Meridional component

To understand the degree of variance at each depth, the mean meridional vector at each depth, with its standard deviation, is presented in Table 4. Mean meridional vector data indicates the net direction of water movement at each depth, with negative values indicating southward and positive values indicating northward. The ADCP data suggests that water movement was primarily in a northward direction between 2 m and 26 m and southward from 30 to 110 m (Table 4). By contrast, the Mercator data

product indicated a net northward flow at all depths over the full time series. Seasonal data are available in Appendix 2. Both data sources suggest that the highest variability (shown by the standard deviation (between 0.429-0.237)) occurred above 10 m, with variability steadily decreasing to 0.06 with depth. Variability of the ADCP data was very high between 2 m and 6 m, which is four times higher than that of the Mercator data product. Below 8 m depth, the variability was similar for the ADCP and Mercator data product.

Table 4. Statistical comparison between *in situ* (ADCP) and modelled (Mercator data product) meridional currents (m/s) for all depts. Mean (± standard deviation) and greatest current vector (Max) for the ADCP and the Mercator data product, root-mean-square-error (RMSE), Spearman's rank correlation (ρ), and bias between *in situ* and modelled data.

Depth (m)	Mean (± SD) ADCP	Mean (± SD) Mercator data product	Max ADCP	Max Mercator data product	RMSE	ρ	bias
2	0.176 (± 0.387)	0.096 (± 0.116)	0.741	0.44	0.391	0.19	0.08
4	0.234 (± 0.429)	0.11 (± 0.13)	0.748	0.436	0.445	0.14	0.123
6	0.245 (± 0.414)	0.098 (± 0.117)	-0.749	0.43	0.44	0.1	0.146
8	0.227 (± 0.237)	0.093 (± 0.109)	0.735	0.427	0.286	0.09	0.133
10	0.086 (± 0.09)	0.085 (± 0.106)	0.432	0.424	0.123	0.21	0.001
12	0.059 (± 0.12)	0.084 (± 0.106)	0.427	0.421	0.146	0.19	-0.025
14	0.025 (± 0.115)	0.076 (± 0.104)	0.392	0.418	0.148	0.19	-0.05
16	0.021 (± 0.106)	0.07 (± 0.1)	0.331	0.414	0.141	0.16	-0.048
18	0.018 (± 0.1)	0.065 (± 0.089)	0.316	0.408	0.133	0.14	-0.047
22	0.007 (± 0.092)	0.068 (± 0.08)	0.324	0.392	0.128	0.14	-0.06
26	0 (± 0.086)	0.068 (± 0.074)	0.284	0.297	0.122	0.2	-0.069
30	-0.005 (± 0.082)	0.067 (± 0.071)	0.265	0.291	0.116	0.27	-0.072
34	-0.008 (± 0.079)	0.063 (± 0.072)	0.25	0.297	0.109	0.37	-0.071

Depth (m)	Mean (± SD) ADCP	Mean (± SD) Mercator data product	Max ADCP	Max Mercator data product	RMSE	ρ	bias
40	-0.01 (± 0.075)	0.057 (± 0.067)	0.268	0.289	0.1	0.44	-0.068
48	-0.014 (± 0.073)	0.053 (± 0.065)	0.26	0.279	0.096	0.47	-0.067
56	-0.019 (± 0.071)	0.041 (± 0.073)	0.246	0.264	0.095	0.45	-0.061
66	-0.024 (± 0.068)	0.024 (± 0.067)	0.263	0.21	0.086	0.42	-0.048
78	-0.027 (± 0.064)	0.011 (± 0.066)	0.236	-0.208	0.079	0.42	-0.039
92	-0.027 (± 0.061)	0.015 (± 0.069)	0.234	0.23	0.073	0.55	-0.042
110	-0.026 (± 0.06)	0.017 (± 0.06)	0.193	0.193	0.064	0.65	-0.043

RMSE values were highest at the surface (0.445 at 4 m), but typically decreased with depth (0.064 at 110 m). There was a three-fold decrease in RMSE values between 6 m and 8 m, but very little variation below 10 m. Similar to the ADCP zonal current data, the bias of the meridional current is lower than the standard deviation recorded for the ADCP data (Table 4). Particularly between 10 m and 30 m where the standard deviation is higher, the bias indicates that the Mercator data product is simulating current readings within an acceptable range of the ADCP. On the other hand, correlation was lowest above 10 m and only strengthened below 30 m.

Comparative metrics on meridional vectors in the surface 12 m did not perform well. This is likely due to the high variability in this region, as well as to the poor quality of measured data from the ADCP in this zone due to beam spreading and sound attenuation resulting in decreased echo intensity (Gordon, 1996). As a result, the next part of the section analyses the seasonal patterns at depths below 14 m.

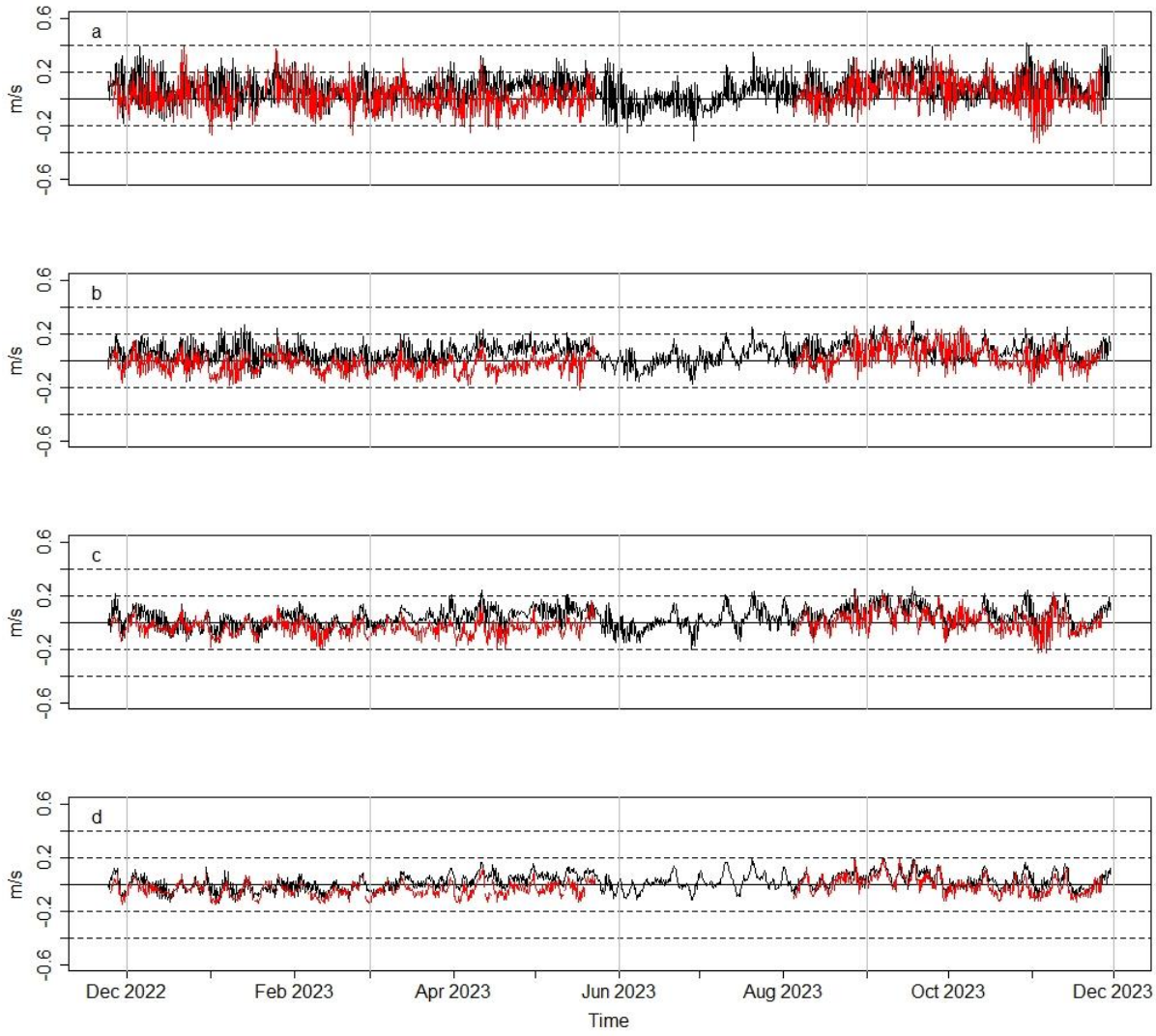

Figure 9. Meridional time series data from the ADCP (red lines) and Mercator data product (black lines) at 14 m (a), 30 m (b), 56 m (c) and 110 m depth (d). A six-hour running mean is applied to the ADCP data. Vertical grey lines denote seasonal splits (starting with summer to the right of Dec 2022), and horizontal dotted lines show breaks between slow (0-0.2 m/s), moderate (0.2-0.4 m/s), and high (0.4-0.6 m/s) current velocities. Negative values indicate a southerly direction, positive values are northerly. These depths were selected for their spread through the water column and for their clarity on the general trends.

Table 5 presents the proportions of time the water at a given depth (14-110 m) in a given season was moving northward or southward, and in which velocity category (slow: 0-0.2 m/s, moderate: 0.2-0.4 m/s, high: and 0.4-0.6 m/s) in the ADCP and the Mercator data product.

In summer, the majority of the slow-moving water measured by the ADCP was flowing southwards (with minor exceptions at depth of 16 m and 18 m). Below 22 m, the current was flowing southwards at slow speeds more than 50% of the time. Moderate speeds were most frequently recorded above 20 m and were more likely to be moving northwards. Moderate currents at depths greater than 30 m were only measured moving southwards. High current speeds in summer were predominantly measured flowing northerly and recorded less than 0.5% of the time. Similarly, the Mercator data product simulated slow and moderate current speed categories reasonably well, but only captured the correct dominant direction 42 and 50% of the time across all depths, respectively (seen in Figure 9-a where the Mercator data product are predominantly above the 0 m/s line and the ADCP data are predominantly below it). The Mercator data product didn't simulate high speeds at any point and over-simulated the frequency of occurrence of northward currents.

In autumn, currents were moving at slow speeds over 90% of the time, with at least 50% of the overall instances being southerly at all depths. Moderate currents were less frequent overall (and at least twice as likely to be moving southerly), but moderate speeds were recorded at all depths. However, high northward velocities were recorded only at a depth of 14 meters, occurring in 0.3% of instances. The Mercator data product once again represented a similar overall instance of speed as the ADCP data

but depicted a conflicting predominant direction for all depths (Figure 9). It incorrectly simulated northward currents at slow speeds and did not simulate instances of moderate southward currents.

The same overall breakdown of current velocities was measured in winter as in autumn, but with different directional patterns. The majority of slow currents were northerly in winter, with an exception at 78 m which was flowing predominantly in a southerly direction. Moderate currents were more common in winter than in autumn, mostly moving northwards, and were present at all depths except 48 m. There were no high velocities recorded in this period. The Mercator data product comparison was limited to August, as this was the only winter month for which ADCP data was available. The Mercator data product captured the predominant direction of slow currents but overrepresented the frequency of northward current instances at all depths. The Mercator data product contained more frequent northward moderate currents at 14, 16 and 34 m and less frequent moderate velocity at all other depths. It never simulated moderate southerly movements.

Between 60 and 80% (depending on the depth) of the spring current instances, were at slow speeds and moving northwards. Higher instances of moderate current velocities were measured in spring compared to the other seasons, between 10 and 20% of the time at depths shallower than 22 m. All moderate currents were moving northwards. The Mercator data product once again captured the overall velocity trends of the spring months. It captured the majority direction of slow speeds well (~70% of the time). The direction of moderate currents represented by the Mercator data product was always in agreement with those recorded by the ADCP with similar magnitudes.

High velocity currents were simulated 0.5% of the time at 14, 16, and 18 m with equal probability of a high velocity event moving northwards and southwards, but never recorded by the ADCP. Once again, the Mercator data product is simulating more northward instances than were measured by the ADCP.

Table 5. Percentage occurrence of current velocity and direction for meridional ADCP (Mercator data product) currents. Current velocity bands (slow: 0-0.2, moderate: 0.2-0.4, high: 0.4-0.6 m/s) in the northward (N (V+)) and southward (S (V-)) direction presented at 14 depths for Summer (1 Dec to 28 Feb), Autumn (1 Mar to 31 May), Winter (1 Jun to 31 Aug), and Spring (1 Sep to 31 Nov). Values in bold indicate the bulk direction for each current velocity band at each depth.

	0-0.2 m/s		**0.2-0.4 m/s**		**0.4-0.6 m/s**	
Depth	**N (V+)**	**S (V-)**	**N (V+)**	**S (V-)**	**N (V+)**	**S (V-)**
Summer						
14	40.34 **(54.54)**	**46.3** (34.09)	**10.79 (11.36)**	2.27 (0)	0 (0)	0 (0)
16	**49.1 (53.35)**	42.73 (36.59)	**5.86 (10.05)**	1.67 (0)	**0.27** (0)	0 (0)
18	**50.4 (59.05)**	43.45 (32.86)	**4.45 (8.07)**	0.83 (0)	**0.27** (0)	0 (0)
22	43.8 **(62.5)**	**51.11** (30.83)	**2.22 (6.66)**	0.83 (0)	0 (0)	0 (0)
26	42.2 **(71.11)**	**55** (25.27)	0.27 **(3.61)**	**2.22** (0)	0 (0)	0 (0)
30	35.5 **(69.72)**	**61.94** (27.22)	0.55 **(3.05)**	**1.38** (0)	0 (0)	0 (0)
34	32.5 **(68.61)**	**66.38** (30.55)	0 **(0.83)**	**0.83** (0)	0 (0)	0 (0)
40	27.7 **(68.61)**	**70.27** (31.11)	0 **(0.27)**	**1.11** (0)	0 (0)	0 (0)
48	28.8 **(63.05)**	**69.72** (36.94)	0 (0)	**1.11** (0)	0 (0)	0 (0)
56	26.4 **(51.81)**	**72.14** (48.18)	0 (0)	**1.39** (0)	0 (0)	0 (0)
66	22.9 (41.62)	**76.25 (58.37)**	0 (0)	**0.55** (0)	0 (0)	0 (0)
78	18.6 (30.83)	**80.55 (68.61)**	0 (0)	**0.27 (0.55)**	0 (0)	0 (0)
92	20.6 (24.23)	**78.83 (75.76)**	0 (0)	0 (0)	0 (0)	0 (0)
110	21.1 (31.75)	**77.99 (68.24)**	0 (0)	0 (0)	0 (0)	0 (0)
Autumn						

Depth	0-0.2 m/s		0.2-0.4 m/s		0.4-0.6 m/s	
	N (V+)	S (V-)	N (V+)	S (V-)	N (V+)	S (V-)
14	42.64 **(73.87)**	**49.84** (19.81)	2.7 **(6.3)**	**4.2** (0)	**0.3** (0)	0 (0)
16	42.3 **(72.37)**	**52.25** (22.22)	1.8 **(5.4)**	**2.4** (0)	0 (0)	0 (0)
18	41.6 **(74.55)**	**53.89** (21.25)	1.19 **(4.19)**	**2.99** (0)	0 (0)	0 (0)
22	39 **(78.97)**	**54.95** (18.01)	1.5 **(3)**	**3.6** (0)	0 (0)	0 (0)
26	32.6 **(82.63)**	**64.07** (15.56)	0.29 **(1.79)**	**2.09** (0)	0 (0)	0 (0)
30	29.6 **(83.83)**	**68.56** (14.67)	0.29 **(1.49)**	**1.19** (0)	0 (0)	0 (0)
34	28.4 **(84.43)**	**69.46** (13.77)	0 **(1.79)**	**0.89** (0)	0 (0)	0 (0)
40	28.7 **(82.63)**	**69.46** (16.16)	0.29 **(1.19)**	**0.59** (0)	0 (0)	0 (0)
48	27.5 **(86.22)**	**72.15** (12.87)	0 **(0.89)**	**0.29** (0)	0 (0)	0 (0)
56	22.4 **(82.93)**	**75.44** (15.86)	0 **(1.19)**	**0.89** (0)	0 (0)	0 (0)
66	22.6 **(82.47)**	**75.83** (17.52)	0 (0)	**0.6** (0)	0 (0)	0 (0)
78	25.5 **(77.47)**	**72.07** (22.52)	0 (0)	**1.2** (0)	0 (0)	0 (0)
92	21.6 **(72.97)**	**76.87** (26.42)	0 **(0.6)**	**0.9** (0)	0 (0)	0 (0)
110	23 **(74.25)**	**75.44** (25.74)	0 (0)	**0.29** (0)	0 (0)	0 (0)
Winter						
14	**53.21 (64.22)**	40.36 (26.6)	**6.42 (9.17)**	0 (0)	0 (0)	0 (0)
16	45.8 **(65.13)**	**45.87** (26.6)	**7.33 (8.25)**	0.91 (0)	0 (0)	0 (0)
18	**50.4 (73.39)**	44.03 (22.93)	**4.58 (3.66)**	0.91 (0)	0 (0)	0 (0)
22	**53.2 (86.23)**	40.36 (12.84)	**3.66 (0.91)**	2.75 (0)	0 (0)	0 (0)
26	**58.7 (88.07)**	37.61 (11)	**1.83 (0.91)**	**1.83** (0)	0 (0)	0 (0)
30	**59.6 (87.15)**	37.61 (11.92)	**1.83 (0.91)**	0.91 (0)	0 (0)	0 (0)
34	**56.8 (87.15)**	39.44 (10.09)	**1.83 (2.75)**	**1.83** (0)	0 (0)	0 (0)
40	**58.7 (88.99)**	39.44 (9.17)	**1.83 (1.83)**	0 (0)	0 (0)	0 (0)
48	**62.3 (87.15)**	37.61 (11.92)	0 **(0.91)**	0 (0)	0 (0)	0 (0)
56	**60.5 (78.89)**	38.53 (20.18)	**0.91 (0.91)**	0 (0)	0 (0)	0 (0)
66	**54.1 (76.14)**	44.03 (22.93)	**1.83 (0.91)**	0 (0)	0 (0)	0 (0)
78	45.8 **(69.72)**	**52.29** (30.27)	**1.83** (0)	0 (0)	0 (0)	0 (0)
92	**50.4 (74.31)**	47.7 (24.77)	**1.83 (0.91)**	0 (0)	0 (0)	0 (0)
110	**55.9 (71.55)**	43.11 (28.44)	**0.91** (0)	0 (0)	0 (0)	0 (0)
Spring						

Depth	0-0.2 m/s		0.2-0.4 m/s		0.4-0.6 m/s	
	N (V+)	S (V-)	N (V+)	S (V-)	N (V+)	S (V-)
14	**52.83 (61.72)**	28.03 (19.94)	**15.36 (18.05)**	3.5 (0)	0 **(0.26)**	0 **(0.26)**
16	**56.4 (64.24)**	27.95 (19.35)	**12.63 (16.12)**	2.95 (0)	0 **(0.26)**	0 **(0.26)**
18	**55.9 (70.96)**	31.45 (16.66)	**11.02 (12.09)**	1.61 (0)	0 **(0.26)**	0 **(0.26)**
22	**56.4 (73.11)**	33.06 (16.93)	**9.13 (9.94)**	1.07 (0)	0 (0)	0 (0)
26	**55.6 (75)**	36.02 (15.86)	**7.25 (9.13)**	1.07 (0)	0 (0)	0 (0)
30	**55.3 (79.03)**	36.82 (15.59)	**6.72 (5.37)**	0.8 (0)	0 (0)	0 (0)
34	**56.1 (77.95)**	39.24 (15.86)	**4.3 (6.18)**	0.26 (0)	0 (0)	0 (0)
40	**58.8 (79.56)**	36.29 (14.24)	**4.83 (6.18)**	0 (0)	0 (0)	0 (0)
48	**54.3 (77.41)**	41.93 (16.39)	**3.49 (6.18)**	0.26 (0)	0 (0)	0 (0)
56	**50 (70.69)**	45.96 (25.8)	**2.68 (3.49)**	1.34 (0)	0 (0)	0 (0)
66	46.7 **(65.59)**	**51.07** (33.87)	0.8 **(0.53)**	**1.34** (0)	0 (0)	0 (0)
78	43.5 **(62.9)**	**54.56** (37.09)	0.8 (0)	**1.07** (0)	0 (0)	0 (0)
92	43.5 **(60.48)**	**54.83** (36.82)	**0.8 (2.68)**	0.53 (0)	0 (0)	0 (0)
110	41.1 **(66.12)**	**58.06** (33.87)	**0.53** (0)	0.26 (0)	0 (0)	0 (0)

In summary, variation of speed and direction of meridional currents was greater in the surface 10 m of the water column. Deviation (in the form of RMSE) decreased with depth while correlation between the Mercator data product and the ADCP measurements improved significantly with depth. Autumn and winter had slow currents 90% of the time, with moderate currents measured at all depths in the water column. In both seasons, the Mercator data product overrepresented northward water movement. Summer also measured primarily slow currents (70% of the time), which the Mercator data product did capture, despite overrepresenting northward flow by 50%. Spring had the highest instance of moderate currents and the best directional match with the Mercator data product. However, the Mercator data product overrepresented northwards flow in general for this comparison period.

4 Discussion

The performance of the Mercator global sea physical analysis and forecasting product, assimilated from satellite observation and *in-situ* measurements by the GLO12v4 engine, was validated in the southern Benguela Upwelling System by comparison with ADCP-derived ocean currents from the same locality. Results of this assessment suggest that the Mercator data product can represent the scale and variability of the magnitude of ocean currents; however, it requires further refinement to capture the sub-daily variability in direction.

4.1 Product performance

Correlation as a metric to compare model outputs to observational data, is normally considered strong at values greater than 0.7 and moderate at values greater than 0.5 (Akoglu, 2018). However, most model validation studies using *in situ* measurements yield correlation values less than 0.7, with anything above 0.5 considered reasonable (Johnson et al., 2007; Sikhakolli et al., 2013; Togneri et al., 2017). Even within this context, the correlation observed between the Mercator data product and the ADCP data in this study was low – 0.31 for the zonal and 0.28 for the meridional velocity components when averaged across all depths. Other studies where direct comparisons have been drawn between a model product and an ADCP data, such as the study of a Regional Ocean Modelling System conducted off the coast of Anglesey (UK) by Togneri et al. (2017), achieved a minimum correlation of 0.86. Similarly, de Pablo et al. (2019) achieved average correlations of 0.63 (zonal) and 0.72 (meridional) in their validation study comparing data from the 3D MOHID water model and an ADCP off the Portuguese coast. The weak correlation between current vectors

simulated by the Mercator data product and those measured by the ADCP in this study, was potentially due in part to the discrepancy in locations. The ADCP is a single point mooring, while the Mercator data product's grid point represents the homogeneous simulated flow for a cell of 5x5 km (Figure 3). The spatial separation between these points could mean that the time of occurrence of events was offset between the ADCP and the Mercator data product and makes correlation a less valuable indicator of performance, though this would require further validation. Positional mismatches are common in most ocean models (Hutchings et al., 2009; Togneri et al., 2017; de Pablo et al., 2019). Furthermore, the ADCP measured with a much higher temporal frequency than that at which the Mercator data product outputs were available. Even though it was time averaged, the ADCP data contains much greater complexity than the sub-daily outputs from the Mercator data product. Analysis of root-mean-square-error (RMSE) and bias suggests that the disparity between currents measured by the ADCP and those represented by the Mercator data product, was much lower than the correlation analysis suggests. These values indicate that current vectors represented by the Mercator data product, were closely aligned with the measured currents – RMSE readings averaged 0.16 (zonal) and 0.21 (meridional) across all depths, bias readings averaged 0.09 (zonal) and 0.02 (meridional) across all depths. The above-mentioned study by Togneri et al. (2017) reported a mean velocity RMSE of 0.20. De Pablo et al. (2019) reported a mean RMSE of 0.079 (zonal) and 0.091 (meridional), and mean bias of 0.005 (zonal) and -0.027 (meridional).

Moderate currents (0.2-0.4 m/s) were measured by the ADCP more frequently in spring and summer than in winter and autumn, which was represented by the Mercator data product at all depths. The ADCP data align well with previous measurements on

current patterns in the nearshore southern Benguela, where speeds have been shown to average 0.05 m/s in winter and 0.2 m/s during summer (Nelson & Hutchings, 1983; Bailey et al., 2001; Largier & Boyd, 2001). In all seasons and at all depths, moderate current events measured by the ADCP were more likely to occur in the zonal vector component than the meridional vector component. This pattern was adequately shown by the Mercator data product aligning with findings from previous studies in the upwelling environment (Largier & Boyd, 2001).

The highest occurrence of slow (0-0.2 m/s) zonal and meridional current events (irrespective of direction) between 14 and 34 m, was measured by the ADCP during the winter period, followed by autumn, then summer, and then spring. The Mercator data product captured this trend well for the zonal vector component at the same depths. Slow meridional vectors represented by the Mercator data product were highest in autumn, followed by winter, summer and lastly spring, for the same depth range (14-34 m). The Mercator data product consistently overrepresented the frequency of occurrence of moderate zonal and meridional currents (irrespective of direction) between 14-26 m in spring, summer, and autumn (by as much as 50%), while underrepresenting the magnitude of moderate zonal and meridional currents in winter (by as much as 60%). High velocity (0.4-0.6 m/s) meridional currents moving northward and southward were represented by the Mercator data product at equal frequencies at these depths (14-26 m) in spring, when none were measured by the ADCP. By contrast, high velocity meridional currents were measured in summer and autumn in the ADCP data. High velocity zonal currents were measured by the ADCP at 14 m, 16 m, and 18 m in summer and autumn, and successfully represented by the Mercator data product. The ADCP measured high zonal currents in spring that were

not contained within the Mercator data product, which simulated high zonal currents in winter when none were measured. In summer the Mercator data product overrepresented the frequency occurrence of slow northwest currents by as much as 30%, whereas southeast currents were measured 40-60% of the time by the ADCP. The greatest disparity of current direction was between 14 and 34 m in the autumn season, where the ADCP measured slow southeast currents for 70% of the season, while the Mercator data product simulated slow northwest currents for 75% of the season. In winter, the Mercator data product represented the same meridional direction as the ADCP, but not the correct zonal direction. The measured current direction in spring was well represented by the Mercator data product. The bulk direction for moderate currents represented at these depths (14 and 34 m) by the Mercator data product, was in alignment with those measured by the ADCP for all seasons. However, Mercator data product did not capture the full complexity of the water movement, as it never represented the observed southerly or easterly moderate currents which were measured by the ADCP <4% of the time in all seasons in these waters (seen in Fawcett, Pitcher & Shillington (2008)).

At depths below 40 m there is very little seasonal variability in the current direction, irrespective of magnitude. The Mercator data product underrepresented moderate meridional currents in autumn and winter, and particularly in summer (~1% difference). In spring, 3% more moderate currents were measured by the ADCP than were simulated by the Mercator data product. At depths greater than 40 m, high zonal or meridional current events occurred <0.01% of the time, as measured by the ADCP or contained within the Mercator data product for any given season. In summer the Mercator data product overrepresented the frequency occurrence of slow northwest

currents by >50% at depths between 40-66 m. In summer, water below this (78-110 m) represented by the Mercator data product contains a slow southeast flow within 10% of the frequency occurrence measured by the ADCP. The Mercator data product represented the greatest disparity of current direction for these depths in the autumn season, where the ADCP measured slow southeast currents for 70% of the season and the Mercator data product simulated slow northwest currents for 70% of the season. In winter, the Mercator data product represented the same bulk meridional direction as the ADCP data, but not the correct zonal direction. In addition, the ADCP measured light upwelling at depth (below 78 m), while the Mercator data product contained a majority offshore movement of water. During the spring period, the Mercator data product represented the complexity of current directions measured by the ADCP at 40-66 m depths well, but this was not the case for waters below 78 m. The Mercator data product represented a bulk direction for the moderate currents in all seasons that was aligned with the ADCP data. However, it did not capture the full complexity of the water movement, as it never contained southerly or easterly moderate currents which were measured by the ADCP <2% of the time below 40 m in all seasons.

4.2 Regional parameters

Daily inertial current oscillations in the full water column were measured by the ADCP and were represented by the Mercator data product for both zonal and meridional vector components (also described by Shillington (1996), Shannon (2009), and Fearon et al. (2023)). In these oscillations, currents in the top 34 m typically exhibit a 12-hour period of strong north-westerly flow, followed by a 12-hour period of weak south-easterly flow. These are characterized by ‘peak speed bursts’ driven by the land-

sea breeze (LSB) in the order of magnitude of 0.1-0.4 m/s in summer and dampened during the winter period (0.05-0.3 m/s). Zonal currents at depths deeper than 40 m exhibited a weak (maximum range of 0.1 m/s) daily oscillation, the periodicity of which mirrored the surface currents and included a 12-hour period of relatively strong easterly flow followed by a 12-hour period of weak westerly flow that strengthened during extreme wind events (Shannon 2009). Meridional current oscillations in waters below 78 m were measured by the ADCP and were represented by the Mercator data product consistently (daily) during the summer months, and less frequently (weekly) during the winter months. The onset of these daily oscillations as measured by the ADCP and represented by the Mercator data product, match in date and time. However, while the daily instance of oscillation is consistent and similarly measured by the ADCP and represented by the Mercator data product, surface currents contained within the Mercator data product were less likely to shift through a full 180° and only completed an oscillation cycle during extreme wind events that were prevalent only during the summer months. Irrespective of the season, the ADCP measured these oscillations more consistently with daily 180° shifts in the surface current direction. The Mercator data product (like most climate scale models) does include LSB within its atmospheric forcing, likely resulting in the incomplete consideration of sheer and rotational friction of air-sea dynamics and so underrepresenting the full shifts (Fearon et al., 2023).

The region of the southern Benguela upwelling system where the ADCP was deployed, experiences moderate-high monthly wind stress, which drives a proportional amount of upwelling (Shannon, 2009). South of the Lüderitz upwelling cell during seasons of upwelling, an inner-shelf poleward flowing counter current is

generally present towards the bottom of the water column, which experiences interannual and seasonal variability (Shillington, 1996; Fawcett, Pitcher & Shillington, 2008; Kirkman et al., 2016). This slow poleward countercurrent was measured in summer and autumn by the ADCP, with 70% of the measured events being slow and southerly at depths greater than 40 m in these seasons, but was absent as a dominant bulk flow in winter and spring. The counter current below 40 m averaged 0.05 m/s southeast in summer and autumn, which aligns with previously reported speeds of 0.05-0.08 m/s for this current (L. V Shannon, 2009). Current reversals occur when the prevailing equatorward upwelling-favourable winds relax, or could be a result of the surfacing of the undercurrent driven by a strong negative winds stress curl (often in the summer and autumn seasons) (Fennel et al., 2012). This seasonal counter current was only weakly represented for the summer months by the Mercator data product (60% occurrence on average below 40 m compared to the 75% occurrence measured by the ADCP), and very weakly represented in autumn (20% occurrence on average below 40 m compared to the 70% occurrence measured by the ADCP).

4.3 Implications

Recurring global and regional atmospheric events like the El Niño Southern Oscillation (ENSO) or the Benguela Niño events, shift prevalent ocean currents and result in extreme weather conditions in the Benguela Upwelling System (Shannon et al., 1986; Rouault & Tomety, 2022). The Benguela Niño shifts fishing grounds, changes ocean productivity, and changes rainfall patterns (Illig & Bachèlery, 2023). Decreases in fisheries' catches and variable rainfall impact food availability, with direct consequences for neighbouring dependent countries (South Africa, Namibia, and Angola in this case) (Illig & Bachèlery, 2023; Vigil & Booker, 2023). These anomalous

conditions have a build-up time, with currents starting to weaken before shifting direction, and circulation patterns change completely. Validated, regionally modelled current data throughout the water column from the Mercator data product could be used as input for predictive forecasting of extreme weather events. This would benefit environmental and socio-economic governance, by allowing key decision makers the ability to implement strategies proactively rather than reactively. It would also enable them to better protect the food security of their citizens and the job security of their fishing sectors. The Mercator data product showed the seasonal shifts in current intensity and direction measured by the ADCP, which are driven by the data sources fed into the Mercator data product. It is likely then, that the Mercator data product would also simulate anomalous events like the Benguela Niño, which are driven by atmospheric changes and occur over long-time scales (months to years). This would make it a useful tool in this situation.

One of the ways to reduce ship fuel consumption (saving on resources and greenhouse gas emissions) is to optimise ship speed and trajectory by using current data in route planning. When ocean currents are taken into consideration in ship optimisation models, the difference between estimated ‘speed over ground’ (SOG) and measured SOG decreases by 3%, allowing for more accurate optimization parameters (Yang et al., 2020). The direction and speed of surface ocean currents, and the influence of waves, are factors that are widely considered within ship voyage emission optimisation studies (Lo & McCord, 1995; Atodiresei et al., 2019; Wang, Mao & Eriksson, 2019; Taskar & Andersen, 2020; Yu et al., 2021). The Mercator data product captures the speed of zonal currents as well as the speed and direction of meridional ocean currents in the nearshore environment of a region. Ship optimization

models can use regionally validated current vectors from the Mercator data product, especially in the southern Benguela Upwelling System, since most maritime transit in the region is moving north-south (Walker, 1987). Access to globally available current data from the Mercator data product provides the shipping industry with the ability to plan and schedule routes, optimising fuel consumption and shipping time.

Oil spill modelling requires validated ocean current vectors for both vertical and horizontal (three-dimensional) domains. Processes such as turbulent mixing and buoyant forcing (vertical currents and stratification) transport oil droplets up and down in the water column, while ocean currents, waves, and winds transport oil horizontally. These horizontal transport mechanisms are the most crucial elements within oil spill models (Keramea et al., 2021). An ocean circulation model's ability to represent accurately horizontal transport mechanisms at the surface, is crucial in simulating real-time particle transport (Sperrevik, Röhrs & Christensen, 2017). Due to the decreased quality of measurements made by upwards-facing ADCP devices in the surface water (due to beam spreading and sound attenuation resulting in decreased echo intensity (Gordon, 1996)), a downwards-facing ADCP would provide more valuable data with which to validate the surface currents simulated by the Mercator data product. Within this validation study, the performance of the Mercator data product in the surface waters was not clear, so the suitability of the Mercator data product in oil spill modelling is unknown. The fact that the Mercator data product does not include vertical velocity, waves or tidal input in the current GLO12v4 model, further weakens its use in oil spill modelling.

Offshore mining activities directly impact the water column with the direct removal and lifting of benthic substrate to the surface, leading to the formation of sediment plumes in the water column because of sediment trailing deposits after the screening process. For this reason, ‘plume models’ have been developed to predict the extent and duration of sediment plumes and to assist in delineating affected habitats (e.g. Boschen et al., 2013; Jankowski & Zielke, 2001; Thiel, 2001). Plume modelling requires information on the composition of the suspended sediments (principally the particle size distribution), sea water temperature and salinity, and the speed and direction of ocean currents at and above the sea floor (Spearman et al., 2020). If water movement in an area is dominated by internal tide-generated currents, subtidal current readings at depth are required to generate an accurate plume model (Spearman et al., 2020). Currents represented by the Mercator data product correlated more strongly with measurements made by the ADCP as depth increased, and were a superior fit in waters below 40 m. This implies that the Mercator data product would be well suited for use in plume modelling in this region as it captures the shear of the current.

Ocean currents are not a major component of fishing ground prediction models in the way temperature or salinity are (Klemas, 2013). This is likely due to the historic accuracy of predicting temperature and salinity, compared to water movement, as well as the biological properties of fishes and their response to water movement. The complexity of ocean processes means that more complex fish location prediction models are often more accurate in the long run. For example, including daily ocean current speed and direction data from the Mercator data product in northern Chile, improved the fishing ground prediction model for *Engraulis ringens* by 2%, a proportion that could improve with further improvements in ocean current forecasting capabilities

and increasing complexity in fishery ground prediction models (Armas, Arancibia & Neira, 2022). Within the southern Benguela region, there are complex connections between fish species that spawn on the Agulhas banks and their feeding grounds on the west coast of South Africa and Namibia, with larval transport being strongly influenced by the currents (Grote et al., 2007). A current simulation model that performs well with bulk flow direction, like the Mercator, could inform the fisheries industry what proportion of larval recruits are transported to optimal feeding grounds and what proportion are taken out into the open ocean and likely lost. This type of analysis could enhance our ability to predict yield for each recruiting year.

4.4 Future works/caveats

High velocity current occurrences in the typically slow-moving Benguela current system are typically driven by strong upwelling events due to high wind stress curl (Fennel, 1999). The discharge of fresh, turbid water into the Southern Benguela system by the Orange River can also influence offshore flow during high flood years (Lett et al., 2007), which adds complexity, as the catchment area for the Orange River covers four countries (South Africa, Lesotho, Botswana, and Namibia (Jeleni & Mare, 2007)), and discharge from this catchment is significant (mean annual runoff = 5 500-11 000 million m^3/year). Compared to the global coverage of the Mercator data product, a single-location mooring has low temporal resolution against which to validate the functioning of the data product in capturing the horizontal structure and patterns of the currents. An array of moorings covering a grid location would allow for a more complete comparison between measured and modelled data and further validate the ability of the Mercator data product to simulate ocean currents in the region. The Mercator data product also does not include tidal inputs or vertical velocity,

which is a potential shortcoming in a region with such productive upwelling. Future works that compare the vertical structure of the water column specifically during upwelling events, would be beneficial.

The approach this study took was motivated by high vessel traffic in the area which necessitated an upwards-facing ADCP configuration. A downwards-facing ADCP would have greater certainty of currents measured in the surface waters (<10 m), which would have allowed for a better comparison of this highly dynamic environment and the simulation capabilities of the Mercator data product. Furthermore, the ADCP was only deployed for one (August) of the three winter months, which limited the time series available for comparison. A more complete time series would be valuable in a region like the nearshore component of the southern Benguela Upwelling System, which is known to have high seasonality.

5 Conclusion

Knowledge of global ocean currents is fundamental to the ocean and its utilisation, but current vector datasets are difficult to acquire through direct measurements on the scale at which they are needed, consequently leading to an increased need for developing and validating global ocean models (Fossette et al., 2012). Having freely available forecasting products is highly valuable. Validation against *in situ* measurements like those made using an ADCP in the southern Benguela Upwelling System are important to understand the degree of accuracy global current models have on a regional scale. The modelled and measured data were not strongly correlated at any depth, likely due to the spatial and temporal differences between the

two datasets. However, the measures of difference (RMSE and bias) suggest that the Mercator data product was representing current values within the natural variability of the system, as measured by the ADCP, reasonably well. The Mercator data product captured the seasonal variability in magnitude measured by the ADCP throughout the water column. The pattern and timing of the daily harmonic oscillations measured by the ADCP were contained within the Mercator data product, even though the complexity of the direction of bulk flow measured by the ADCP was not well represented. The poleward counter current measured in the bottom waters by the ADCP during summer and autumn, was also captured by the Mercator data product in summer. Current vectors from the Mercator data product can be used to force, or be assimilated into, finer-scale partial tracking models for offshore mining impact assessments, oil spill mitigation plans, fishery yield estimations, maritime transit planning, and climate analyses within the Benguela Upwelling System.

References

Abdallah, I.M. & Chantsev, V.Y. 2022. Modeling marine oil spill trajectory and fate off Hurghada, Red Sea coast, Egypt. *Egyptian Journal of Aquatic Biology & Fisheries*. 26(6):41–61.

Akoglu, H. 2018. User's guide to correlation coefficients. *Turkish Journal of Emergency Medicine*. 18(3):91–93. DOI: 10.1016/j.tjem.2018.08.001.

Armas, E., Arancibia, H. & Neira, S. 2022. Identification and Forecast of Potential Fishing Grounds for Anchovy (Engraulis ringens) in Northern Chile Using Neural Networks Modeling. *Fishes*. 7(4):204. DOI: 10.3390/fishes7040204.

Atodiresei, D., Nedelcu, A.-T., Toma, A., Lupu, S., Rossemary Apetroaei, M. & Aptula, A. 2019. Optimization the navigation route from Singapore to Santos by using the ship`s software and processing the hydrometherological parameters received in real time. *Journal of Physics: Conference Series*. 1297(1):012027. DOI: 10.1088/1742-6596/1297/1/012027.

Bailey, G., Boyd, A., Duncombe Rae, C., Mitchell-Innes, B. & van der Plas, A. 2001. Synthesis of marine science research in the Benguela Current system during cruises linked to the BENEFIT training programme in 1999. *South African Journal of Science*. 97(5):271–274.

Barbour, N., Bailey, H., Fagan, W.F., Mustin, W., Baboolal, V., Casella, F., Candela, T., Gaspar, P., et al. 2023. Satellite Tracking of Head-Started Juvenile Green Turtles (Chelonia mydas) Reveals Release Effects and an Ontogenetic Shift. *Animals*. 13(7):1218. DOI: 10.3390/ani13071218.

Baxley, W.E. 2013. Ocean current measurements: Challenges and opportunities in the Florida Current. Masters of Science. Nova Southeastern University.

Bertolini, C. & Pastres, R. 2023. Understanding the influence of swarming timing on the dispersal of Ostrea edulis larvae in the Northern Adriatic Sea. *Open Research Europe*. 3:212. DOI: 10.12688/openreseurope.16776.1.

Blockley, E.W., Martin, M.J. & Hyder, P. 2012. Validation of FOAM near-surface ocean current forecasts using Lagrangian drifting buoys. *Ocean Science*. 8(4):551–565. DOI: 10.5194/os-8-551-2012.

Boschen, R.E., Rowden, A.A., Clark, M.R. & Gardner, J.P.A. 2013. Mining of deep-sea seafloor massive sulfides: A review of the deposits, their benthic communities, impacts from mining, regulatory frameworks and management strategies. *Ocean & Coastal Management*. 84:54–67. DOI: 10.1016/j.ocecoaman.2013.07.005.

Calvino, C., Dabrowski, T. & Dias, F. 2022. A study of the sea level and current effects on the sea state in Galway Bay, using the numerical model COAWST. *Ocean Dynamics*. 72(11–12):761–774. DOI: 10.1007/s10236-022-01532-w.

Chao, Y., Zhang, H., Chao, Y., Farrara, J.D., Armenta, K.J., Walter, R.K., Centurioni, L., Rudnick, D., et al. 2018. Development, implementation, and validation of a California coastal ocean modeling, data assimilation, and forecasting system. *Deep-Sea Research Part II: Topical Studies in Oceanography*. 151:49–63. DOI: 10.1016/j.dsr2.2017.04.013.

Chávez-Castrillón, F., Marchán-Hernánez, S., Ivaldi, R. & Sciavicco, G. 2023. Fourier-based optimization for multivariate spatial-temporal regression model in chlorophyll-a presence prediction around Galápagos Islands. *Revista InGenio*. 6(1):31–43. DOI: 10.18779/ingenio.v6i1.561.

Dalsøren, S.B., Albretsen, J. & Asplin, L. 2020. New validation method for hydrodynamic fjord models applied in the Hardangerfjord, Norway. *Estuarine, Coastal and Shelf Science*. 246:107028. DOI: 10.1016/j.ecss.2020.107028.

Demir, S. 2022. Comparison of Normality Tests in Terms of Sample Sizes under Different Skewness and Kurtosis Coefficients. *International Journal of Assessment Tools in Education*. 9(2):397–409. DOI: 10.21449/ijate.1101295.

Dohan, K., Lumpkin, R. & Maximenko, N. 2014. Measuring the global ocean surface circulation with satellite and in situ observations Investigating the Variability of Sea Level in the sub-Arctic and Arctic Seas View project Impact of Preferred Eddy Tracks on Tracers in Eastern Boundary Upwelling Systems of the Pacific Ocean View project. Available: https://www.researchgate.net/publication/229024624.

Erlandson, J.M. & Fitzpatrick, S.M. 2006. Oceans, Islands, and Coasts: Current Perspectives on the Role of the Sea in Human Prehistory. *The Journal of Island and Coastal Archaeology*. 1(1):5–32. DOI: 10.1080/15564890600639504.

FAO. 2022. *The State of World Fisheries and Aquaculture 2022. Towards Blue Transformation*. FAO. DOI: 10.4060/cc0461en.

Fawcett, A.L., Pitcher, G.C. & Shillington, F.A. 2008. Nearshore currents on the southern Namaqua shelf of the Benguela upwelling system. *Continental Shelf Research*. 28(8):1026–1039. DOI: 10.1016/j.csr.2008.02.005.

Fearon, G., Herbette, S., Cambon, G., Veitch, J., Meynecke, J.-O. & Vichi, M. 2023. The land-sea breeze influences the oceanography of the southern Benguela upwelling system at multiple time-scales. *Frontiers in Marine Science*. 10. DOI: 10.3389/fmars.2023.1186069.

Fennel, W. 1999. Theory of the Benguela Upwelling System. *Journal of Physical Oceanography*. 29(2):177–190. DOI: 10.1175/1520-0485(1999)029<0177:TOTBUS>2.0.CO;2.

Fennel, W., Junker, T., Schmidt, M. & Mohrholz, V. 2012. Response of the Benguela upwelling systems to spatial variations in the wind stress. *Continental Shelf Research*. 45:65–77. DOI: 10.1016/j.csr.2012.06.004.

Finke, G., Gee, K., Gxaba, T., Sorgenfrei, R., Russo, V., Pinto, D., Nsiangango, S.E., Sousa, L.N., et al. 2020. Marine Spatial Planning in the Benguela Current Large Marine Ecosystem. *Environmental Development*. 36. DOI: 10.1016/j.envdev.2020.100569.

Fofonoff, N. & Millard, R. 1983. Algorithms for computation of fundamental properties of seawater. *UNESCO technical papers in marine science*. 44:1–58. DOI: 10.25607/OBP-1450.

Fossette, S., Putman, N., Lohmann, K., Marsh, R. & Hays, G. 2012. A biologist's guide to assessing ocean currents: a review. *Marine Ecology Progress Series*. 457:285–301. DOI: 10.3354/meps09581.

Glantz, M.H., Naranjo-Diaz, L., Ye, Q. & Pierce, G.E. 2022. Mainstreaming the Full ENSO: Linking Present Weather and Future Climate. *International Journal of Disaster Risk Science*. 13(6):829–841. DOI: 10.1007/s13753-022-00459-6.

Gordon, R.L. 1996. *Principles of Operation A Practical Primer Second Edition for Broadband ADCPs in writing from RD Instruments*. San Diego.

Grimes, C.B. 2001. Fishery Production and the Mississippi River Discharge. *Fisheries*. 26(8):17–26. DOI: 10.1577/1548-8446(2001)026<0017:fpatmr>2.0.co;2.

Gross, M.G. 1977. *Oceanography A view of the Earth*. Second ed. Englewood Cliffs, New Jersey: Prentice-Hall Inc.

Grote, B., Ekau, W., Hagen, W., Huggett, J.A. & Verheye, H.M. 2007. Early life-history strategy of Cape hake in the Benguela upwelling region. *Fisheries Research*. 86(2–3):179–187. DOI: 10.1016/j.fishres.2007.06.003.

Häfner, D., Nuterman, R. & Jochum, M. 2021. Fast, Cheap, and Turbulent—Global Ocean Modeling With GPU Acceleration in Python. *Journal of Advances in Modeling Earth Systems*. 13(12). DOI: 10.1029/2021MS002717.

Hamukuaya, H. 2020. Benguela Current Convention supports ecosystem assessment and management practice. *Environmental Development*. 36. DOI: 10.1016/j.envdev.2020.100574.

Hatje, V., Andrade, R.L.B., Oliveira, C.C. de, Polejack, A. & Gxaba, T. 2021. Pollutants in the South Atlantic Ocean: Sources, Knowledge Gaps and Perspectives for the Decade of Ocean Science. *Frontiers in Marine Science*. 8. DOI: 10.3389/fmars.2021.644569.

Holland, W.R. 1978. The Role of Mesoscale Eddies in the General Circulation of the Ocean—Numerical Experiments Using a Wind-Driven Quasi-Geostrophic Model. *Journal of Physical Oceanography*. 8(3):363–392. DOI: 10.1175/1520-0485(1978)008<0363:TROMEI>2.0.CO;2.

Hutchings, L., van der Lingen, C.D., Shannon, L.J., Crawford, R.J.M., Verheye, H.M.S., Bartholomae, C.H., van der Plas, A.K., Louw, D., et al. 2009. The Benguela Current: An ecosystem of four components. *Progress in Oceanography*. 83(1–4):15–32. DOI: 10.1016/j.pocean.2009.07.046.

Illig, S. & Bachèlery, M. Lou. 2023. The 2021 Atlantic Niño and Benguela Niño Events: external forcings and air–sea interactions. *Climate Dynamics*. 62:679–702. DOI: 10.1007/s00382-023-06934-0.

Jankowski, J.A. & Zielke, W. 2001. The mesoscale sediment transport due to technical activities in the deep sea. *Deep Sea Research Part II: Topical Studies in Oceanography*. 48(17–18):3487–3521. DOI: 10.1016/S0967-0645(01)00054-6.

Jeleni, A. & Mare, H. 2007. *Orange River Integrated Water Resources Management Plan Report: Review of Existing Infrastructure in the Orange River Catchment*.

Johnson, E.S., Bonjean, F., Lagerloef, G.S.E., Gunn, J.T. & Mitchum, G.T. 2007. Validation and error analysis of OSCAR sea surface currents. *Journal of Atmospheric and Oceanic Technology*. 24(4):688–701. DOI: 10.1175/JTECH1971.1.

Justice, C., Belward, A., Morisette, J., Lewis, P., Privette, J. & Baret, F. 2000. Developments in the "validation" of satellite sensor products for the study of the land surface. *International Journal of Remote Sensing*. 21(17):3383–3390. DOI: 10.1080/014311600750020000.

Kacev, D. & Lewison, R.L. 2016. Satellite Remote Sensing in Support of Fisheries Management in Global Oceans. *Earth Science Satellite Applications*. 207–222. DOI: 10.1007/978-3-319-33438-7_8.

Kainge, P., Kirkman, S.P., Estevão, V., van der Lingen, C.D., Uanivi, U., Kathena, J.N., van der Plas, A., Githaiga-Mwicigi, J., et al. 2020. Fisheries yields, climate change, and ecosystem-based management of the Benguela Current Large Marine Ecosystem. *Environmental Development*. 36(100567). DOI: 10.1016/j.envdev.2020.100567.

Kasahara, A. 1974. Various Vertical Coordinate Systems Used for Numerical Weather Prediction. *Monthly Weather Review*. 102:509–522. DOI: 10.1175/1520-0493(1974)102<0509:VVCSUF>2.0.CO;2.

Keramea, P., Spanoudaki, K., Zodiatis, G., Gikas, G. & Sylaios, G. 2021. Oil Spill Modeling: A Critical Review on Current Trends, Perspectives, and Challenges. *Journal of Marine Science and Engineering*. 9(2):181. DOI: 10.3390/jmse9020181.

Kirkman, S.P., Blamey, L., Lamont, T., Field, J.G., Bianchi, G., Huggett, J.A., Hutchings, L., Jackson-Veitch, J., et al. 2016. Spatial characterisation of the Benguela ecosystem for ecosystem-based management. *African Journal of Marine Science*. 38(1):7–22. DOI: 10.2989/1814232X.2015.1125390.

Klemas, V. 2012. Remote sensing of coastal and ocean currents: An overview. *Journal of Coastal Research*. 28(3):576–586. DOI: 10.2112/JCOASTRES-D-11-00197.1.

Klemas, V. 2013. Fisheries applications of remote sensing: An overview. *Fisheries Research*. 148:124–136. DOI: 10.1016/j.fishres.2012.02.027.

Kristensen, N.M. & Gusdal, Y. 2021. *NorKyst800 model currents validation* . Oslo, Norway. Available: https://www.met.no/publikasjoner/met-report/met-report-2021/_/attachment/download/8b99ea1b-200f-4a09-9eb7-3ada0580e157:56ff9d6c44186aa495be038a1cc5dd84d3ca3f2a/MET-report-02-2021.pdf [2024, January 23].

Largier, J. & Boyd, A. 2001. Drifter observations of surface water transport in the Benguela Current during winter 1999. *South African Journal of SCience*. 97(5):223-229`.

Laurindo, L.C., Mariano, A.J. & Lumpkin, R. 2017. An improved near-surface velocity climatology for the global ocean from drifter observations. *Deep Sea Research Part I: Oceanographic Research Papers*. 124:73–92. DOI: 10.1016/j.dsr.2017.04.009.

Lee Dantzler, H. 1976. Geographic variations in intensity of the North Atlantic and North Pacific oceanic eddy fields. *Deep Sea Research and Oceanographic Abstracts*. 23(9):783–794. DOI: 10.1016/0011-7471(76)90846-9.

Lellouche, J.-M., Le Galloudec, O., Regnier, C., Gennip, S. Van, Law Chune, S., Levier, B., Greiner, E., Drevillon, M., et al. 2022. *Global Production Centre GLO_ANALYSISFORECAST_PHY_001_024 Issue: 1.0*.

Leming, T. 1990. *Satellite imagery analysis/PC data link for directed butterfish fishing*.

Lett, C., Veitch, J., Van Der Lingen, C.D. & Hutchings, L. 2007. Assessment of an environmental barrier to transport of ichthyoplankton from the southern to the northern Benguela ecosystems. *Marine Ecology Progress Series*. 347:247–259. DOI: 10.3354/meps06982.

Lo, H.K. & McCord, M.R. 1995. Routing through dynamic ocean currents: General heuristics and empirical results in the gulf stream region. *Transportation Research Part B: Methodological*. 29(2):109–124.

Loew, A., Bell, W., Brocca, L., Bulgin, C.E., Burdanowitz, J., Calbet, X., Donner, R. V., Ghent, D., et al. 2017. Validation practices for satellite-based Earth observation data across communities. *Reviews of Geophysics*. 55(3):779–817. DOI: 10.1002/2017RG000562.

Lorente, P., Piedracoba, S. & Fanjul, E.A. 2015. Validation of high-frequency radar ocean surface current observations in the NW of the Iberian Peninsula. *Continental Shelf Research*. 92:1–15. DOI: 10.1016/j.csr.2014.11.001.

Lorente, P., Rubio, A., Reyes, E., Solabarrieta, L., Piedracoba, S., Tintoré, J. & Mader, J. 2023. *High-frequency radar-derived coastal upwelling index*. DOI: 10.5194/sp-1-osr7.

Lv, A., Fan, L. & Zhang, W. 2022. Impact of ENSO Events on Droughts in China. *Atmosphere*. 13(11):1764. DOI: 10.3390/atmos13111764.

Madec, G. & NEMO team. 2016. NEMO ocean engine.

Madec, G., Delecluse, P., Imbard, M. & Lévy, C. 1998. *OPA 8.1 Ocean General Circulation Model reference manual*. Available: https://www.researchgate.net/publication/243055542.

Mesinger, F. & Arakawa, A. 1976. *Numerical methods used in atmospheric models*. V. 1. Global Atmospheric Research Programme.

Moloney, C.L. 1992. Simulation studies of trophic flows and nutrient cycles in Benguela upwelling foodwebs. *South African Journal of Marine Science*. 12(1):457–476. DOI: 10.2989/02577619209504718.

Myers, D.G. 1990. An application of satellite-derived sea surface temperature data to the Australian fishing industry in near real-time. *International Journal of Remote Sensing*. II(11):2103–2112.

Navalgund, R.R., Jayaraman, V. & Roy, P.S. 2007. Remote sensing applications: An overview. *Current science*. 93(12):1747–1766. Available: https://www.jstor.org/stable/24102069.

Nelson, G. & Hutchings, L. 1983. The Benguela upwelling area. *Progress in Oceanography*. 12(3):333–356. DOI: 10.1016/0079-6611(83)90013-7.

Nguyen, S., Fu, X., Ogawa, D. & Zheng, Q. 2023. An application-oriented testing regime and multi-ship predictive modeling for vessel fuel consumption prediction. *Transportation Research Part E: Logistics and Transportation Review*. 177:103261. DOI: 10.1016/j.tre.2023.103261.

Njutapvoui, N.F., Achab, M., Stieglitz, T., Rudant, J.P., Yap, L., Chouto, S., Tomedi, E.M. & Onguéné, R. 2023. Coastal Vulnerability Assessment in Central Africa-Integration of Earth Observation Technologies and Multi-Criteria Analysis. *SSRN*. (December, 21).

Nortek Group. 2017. *Signature Principles of Operation*. Bærum.

Nortek Group. 2022. *Signature Series Operations Manual*. Bærum.

de Pablo, H., Sobrinho, J., Garcia, M., Campuzano, F., Juliano, M. & Neves, R. 2019. Validation of the 3D-MOHID hydrodynamic model for the Tagus coastal area. *Water* . 11(8). DOI: 10.3390/w11081713.

Pak, G., Lee, K.-J., Lee, S.-W., Jin, H. & Park, J.-H. 2023. Quantification of the extremely intensified East Korea Warm Current in the summer of 2021: offshore and coastal variabilities. *Frontiers in Marine Science*. 10. DOI: 10.3389/fmars.2023.1252302.

Paolo, F., Kroodsma, D., Raynor, J., Hochberg, T., Davis, P., Cleary, J., Marsaglia, L., Orofino, S., et al. 2024. Satellite mapping reveals extensive industrial activity at sea. *Nature*. 625(7993):85–91. DOI: 10.1038/s41586-023-06825-8.

Qiu, C., He, B., Wang, D., Zou, Z. & Tang, H. 2023. Mechanisms of a shelf submesoscale front in the northern South China Sea. *Deep Sea Research Part I: Oceanographic Research Papers*. 202:104197. DOI: 10.1016/j.dsr.2023.104197.

Ragoasha, N., Herbette, S., Cambon, G., Veitch, J., Reason, C. & Roy, C. 2019. Lagrangian pathways in the southern Benguela upwelling system. *Journal of Marine Systems*. 195:50–66. DOI: 10.1016/j.jmarsys.2019.03.008.

Rouault, M. & Tomety, F.S. 2022. Impact of El Niño-Southern Oscillation on the Benguela Upwelling. *Journal of Physical Oceanography*. 52(10):2573–2587. DOI: 10.1175/JPO-D-21.

Santos, A. & Fiuza, A. 1992. Supporting the Portuguese fisheries with satellites. In *Proceedings of the European International Space Year Conference 1992 on ``Space in the Service of the Changing Earth''*. V. 2. Munich, Germany: European Space Agency. 663–668.

Semtner, A. 1995. Modeling Ocean Circulation. *Science*. 269(5229):1379–1385. DOI: 10.1126/science.269.5229.1379.

Shannon, L. V. 2009. Benguela Current. In *Ocean Currents*. 2nd ed. J.H. Steele, S.A. Thorpe, & K.K. Turekian, Eds. San Diego: Academic Press. 23–34.

Shannon, V. 2006. A Plan Comes Together. In *Large Marine Ecosystems*. V. 14. V. Shannon, G. Hempel, P. Malanotte-Rizzoli, C. Moloney, & J. Woods, Eds. 3–10. DOI: 10.1016/s1570-0461(06)80006-6.

Shannon, L. V, Boyd, A.J., Brundrie, G.B. & Taunton-Clarki, J. 1986. On the existence of an El Nifto-type phenomenon in the Benguela System. *Journal of Marine Research*. 44:495–520. Available: https://elischolar.library.yale.edu/.

Shillington, Fap.E. 1996. *Measurement and analysis of wind and current meter data*. Cape Town.

Sikhakolli, R., Sharma, R., Basu, S., Gohil, B.S., Sarkar, A. & Prasad, S.R. 2013. Evaluation of OSCAR ocean surface current product in the tropical Indian Ocean using in situ data. *Journal of Earth System Science*. 122(1):187–199. Available: www.oscar.noaa.gov.

Spearman, J., Taylor, J., Crossouard, N., Cooper, A., Turnbull, M., Manning, A., Lee, M. & Murton, B. 2020. Measurement and modelling of deep sea sediment plumes and implications for deep sea mining. *Scientific Reports*. 10(1). DOI: 10.1038/s41598-020-61837-y.

Sperrevik, A.K., Röhrs, J. & Christensen, K.H. 2017. Impact of data assimilation on Eulerian versus Lagrangian estimates of upper ocean transport. *Journal of Geophysical Research: Oceans*. 122(7):5445–5457. DOI: 10.1002/2016JC012640.

Sudhan Saravana Prabahar, N., Fredriksson, S., Broström, G. & Bergqvist, B. 2022. Experimental Validation of Numerical Simulation of Tidal Power Plants (Deep Green) using ADCP Measurements. In *EGU General Assembly*. Vienna, Austria. EGU22-12664. DOI: 10.5194/egusphere-egu22-12664.

Taskar, B. & Andersen, P. 2020. Benefit of speed reduction for ships in different weather conditions. *Transportation Research Part D: Transport and Environment*. 85:102337. DOI: 10.1016/j.trd.2020.102337.

Thiel, H. 2001. Evaluation of the environmental consequences of polymetallic nodule mining based on the results of the TUSCH Research Association. *Deep Sea Research Part II: Topical Studies in Oceanography*. 48(17–18):3433–3452. DOI: 10.1016/S0967-0645(01)00051-0.

Togneri, M., Lewis, M., Neill, S. & Masters, I. 2017. Comparison of ADCP observations and 3D model simulations of turbulence at a tidal energy site. *Renewable Energy*. 114:273–282. DOI: 10.1016/j.renene.2017.03.061.

Treguier, A.M. 2006. Models of the Ocean: Which Ocean? In *Ocean Weather Forecasting*. E. Chassignet & Verron J, Eds. Berlin/Heidelberg: Springer-Verlag. 75–108. DOI: 10.1007/1-4020-4028-8_3.

Veitch, J., Hermes, J., Lamont, T., Penven, P. & Dufois, F. 2018. Shelf-edge jet currents in the southern Benguela: A modelling approach. *Journal of Marine Systems*. 188:27–38. DOI: 10.1016/j.jmarsys.2017.09.003.

Vigil, A.J.E. & Booker, J.D. 2023. Building national disaster resilience: assessment of ENSO-driven disasters in Peru. *Disaster Resilience in the Built Environment*. 14(4):423–433. DOI: 10.1108/IJDRBE-10-2022-0102.

Walker, N.D. 1987. Interannual sea surface temperature variability and associated atmospheric forcing within the Benguela system. *South African Journal of Marine Science*. 5(1):121–132. DOI: 10.2989/025776187784522108.

Wang, G.-G., Cheng, H., Zhang, Y. & Yu, H. 2023. ENSO analysis and prediction using deep learning: A review. *Neurocomputing*. 520:216–229. DOI: 10.1016/j.neucom.2022.11.078.

Wang, H., Mao, W. & Eriksson, L. 2019. A Three-Dimensional Dijkstra's algorithm for multi-objective ship voyage optimization. *Ocean Engineering*. 186:106131. DOI: 10.1016/j.oceaneng.2019.106131.

Wang, J., Wang, F., Lu, Y., Zhang, H., Ma, Q., Pratt, L.J. & Zhang, Z. 2023. Abyssal Circulation From the Yap-Mariana Junction to the Northern Philippine Basin. *Geophysical Research Letters*. 50(6). DOI: 10.1029/2022GL100610.

Wang, X.T., Liu, H., Lv, Z.F., Deng, F.Y., Xu, H.L., Qi, L.J., Shi, M.S., Zhao, J.C., et al. 2021. Trade-linked shipping CO2 emissions. *Nature Climate Change*. 11(11):945–951. DOI: 10.1038/s41558-021-01176-6.

Washburn, T.W., Turner, P.J., Durden, J.M., Jones, D.O.B., Weaver, P. & Van Dover, C.L. 2019. Ecological risk assessment for deep-sea mining. *Ocean & Coastal Management*. 176:24–39. DOI: 10.1016/j.ocecoaman.2019.04.014.

Williams, A.J., Heron, M.L. & Anderson, S.P. 2008. Technology of water flow measurement represented by thirty years of CMTC. In *OCEANS 2008*. IEEE. 1–8. DOI: 10.1109/OCEANS.2008.5289435.

Yamanaka, I., Ito, S., Niwa, K., Tanabe, R., Yabuta, Y. & Chikuni, S. 1988. *The Fisheries Forecasting System in Japan for Coastal Pelagic Fish*. Rome: FAO Fisheries.

Yang, L., Chen, G., Zhao, J. & Rytter, N.G.M. 2020. Ship speed optimization considering ocean currents to enhance environmental sustainability in maritime shipping. *Sustainability (Switzerland)*. 12(9). DOI: 10.3390/su12093649.

Yu, H., Fang, Z., Fu, X., Liu, J. & Chen, J. 2021. Literature review on emission control-based ship voyage optimization. *Transportation Research Part D: Transport and Environment*. 93. DOI: 10.1016/j.trd.2021.102768.

Zhang, L., Zhang, L., Shi, Y., Yang, Z., Gong, Q. & Sun, D. 2023. PAHs in the monsoonal open ocean: Homogeneous spatial pattern and wind-driven significant

seasonal variations. *Journal of Hazardous Materials*. 454:131462. DOI: 10.1016/j.jhazmat.2023.131462.

Appendix

Appendix 1. Seasonal statistical comparison between *in situ* (ADCP) and modelled (Mercator data product) zonal currents (m/s) for all depth bins. Mean (± standard deviation) and greatest current vector (Max) for the ADCP and the Mercator data product data, root-mean-square-error (RMSE), Spearman's rank correlation (ρ), and bias comparisons between *in situ* and modelled data.

Depth (m)	Mean (± SD) ADCP	Mean (± SD) Mercator data product	Max ADCP	Max Mercator data product	RMSE	ρ	bias
Summer							
2	0.164 (± 0.262)	-0.146 (± 0.115)	0.709	-0.394	0.413	0.15	0.31
4	-0.09 (± 0.131)	-0.162 (± 0.095)	-0.233	-0.274	0.174	-0.071	0.071
6	0.191 (± 0.275)	-0.14 (± 0.125)	0.727	-0.375	0.415	0.361	0.331
8	0.049 (± 0.16)	-0.141 (± 0.12)	-0.485	-0.419	0.241	0.474	0.19
10	-0.029 (± 0.084)	-0.142 (± 0.121)	-0.45	-0.417	0.155	0.551	0.113
12	-0.032 (± 0.163)	-0.125 (± 0.124)	-0.531	-0.414	0.169	0.552	0.093
14	-0.04 (± 0.118)	-0.114 (± 0.123)	-0.501	-0.411	0.142	0.488	0.074
16	-0.025 (± 0.1)	-0.109 (± 0.117)	-0.451	-0.404	0.145	0.392	0.084
18	-0.011 (± 0.087)	-0.095 (± 0.106)	-0.379	-0.381	0.143	0.236	0.084
22	0.008 (± 0.074)	-0.076 (± 0.091)	-0.231	-0.351	0.142	0.033	0.085
26	0.015 (± 0.064)	-0.057 (± 0.073)	0.174	-0.338	0.118	0.08	0.073
30	0.018 (± 0.057)	-0.042 (± 0.067)	0.158	-0.315	0.102	0.113	0.06
34	0.019 (± 0.052)	-0.029 (± 0.065)	0.15	-0.192	0.09	0.171	0.049
40	0.021 (± 0.046)	-0.017 (± 0.055)	0.178	-0.158	0.073	0.256	0.039
48	0.022 (± 0.042)	-0.015 (± 0.05)	0.179	-0.148	0.067	0.239	0.037
56	0.023 (± 0.041)	-0.008 (± 0.051)	0.179	0.144	0.065	0.23	0.032
66	0.021 (± 0.041)	0.003 (± 0.049)	0.163	0.153	0.057	0.277	0.017
78	0.022 (± 0.039)	0.012 (± 0.056)	0.165	0.188	0.059	0.277	0.009

Depth (m)	Mean (± SD) ADCP	Mean (± SD) Mercator data product	Max ADCP	Max Mercator data product	RMSE	ρ	bias
92	0.023 (± 0.032)	0.024 (± 0.05)	0.129	0.182	0.048	0.36	0
110	0.021 (± 0.025)	0.02 (± 0.033)	0.085	0.095	0.035	0.292	0.001
Autumn							
2	0.088 (± 0.325)	-0.081 (± 0.089)	0.723	-0.326	0.373	0.048	0.17
4	0.001 (± 0.185)	-0.086 (± 0.07)	0.584	-0.261	0.185	0.344	0.088
6	0.068 (± 0.233)	-0.076 (± 0.09)	0.691	-0.257	0.269	0.105	0.144
8	0.013 (± 0.156)	-0.124 (± 0.105)	-0.568	-0.454	0.204	0.378	0.138
10	-0.008 (± 0.076)	-0.119 (± 0.105)	-0.383	-0.452	0.151	0.279	0.11
12	0.012 (± 0.128)	-0.118 (± 0.107)	-0.442	-0.449	0.19	0.251	0.131
14	-0.033 (± 0.106)	-0.108 (± 0.101)	-0.468	-0.445	0.142	0.251	0.075
16	-0.023 (± 0.097)	-0.102 (± 0.097)	-0.437	-0.433	0.138	0.249	0.079
18	-0.015 (± 0.092)	-0.088 (± 0.088)	-0.403	-0.4	0.127	0.258	0.072
22	0 (± 0.08)	-0.075 (± 0.079)	-0.299	-0.389	0.119	0.273	0.075
26	0.01 (± 0.067)	-0.063 (± 0.069)	-0.215	-0.314	0.107	0.282	0.073
30	0.015 (± 0.057)	-0.054 (± 0.062)	0.181	-0.258	0.099	0.293	0.07
34	0.018 (± 0.051)	-0.048 (± 0.058)	0.165	-0.228	0.093	0.253	0.066
40	0.021 (± 0.046)	-0.044 (± 0.055)	0.148	-0.257	0.091	0.171	0.065
48	0.023 (± 0.044)	-0.04 (± 0.054)	0.137	-0.236	0.088	0.224	0.063
56	0.023 (± 0.042)	-0.032 (± 0.056)	0.151	-0.213	0.084	0.206	0.055
66	0.021 (± 0.039)	-0.025 (± 0.052)	0.145	-0.173	0.077	0.154	0.046
78	0.022 (± 0.036)	-0.023 (± 0.051)	0.107	-0.161	0.071	0.235	0.045
92	0.02 (± 0.031)	-0.019 (± 0.045)	0.114	-0.13	0.061	0.281	0.039
110	0.019 (± 0.028)	-0.014 (± 0.036)	0.099	-0.107	0.051	0.319	0.034
Winter							
2	0.123 (± 0.366)	-0.036 (± 0.129)	0.733	-0.255	0.394	0.199	0.159
4	0.027 (± 0.361)	-0.102 (± 0.149)	-0.71	-0.496	0.356	0.401	0.13
6	0.047 (± 0.302)	-0.098 (± 0.134)	0.694	-0.491	0.32	0.371	0.145
8	-0.011 (± 0.137)	-0.08 (± 0.129)	-0.368	-0.489	0.177	0.239	0.068
10	0.07 (± 0.092)	-0.078 (± 0.125)	0.297	-0.487	0.195	0.321	0.149

Depth (m)	Mean (± SD) ADCP	Mean (± SD) Mercator data product	Max ADCP	Max Mercator data product	RMSE	ρ	bias
12	-0.001 (± 0.108)	-0.078 (± 0.119)	-0.31	-0.484	0.138	0.488	0.077
14	-0.024 (± 0.105)	-0.078 (± 0.111)	-0.35	-0.482	0.124	0.44	0.054
16	-0.022 (± 0.102)	-0.079 (± 0.102)	-0.356	-0.479	0.121	0.423	0.057
18	-0.02 (± 0.099)	-0.075 (± 0.077)	-0.357	-0.473	0.112	0.308	0.054
22	-0.016 (± 0.092)	-0.077 (± 0.061)	-0.346	-0.452	0.111	0.205	0.06
26	-0.013 (± 0.083)	-0.078 (± 0.057)	-0.338	-0.339	0.113	0.073	0.064
30	-0.01 (± 0.074)	-0.075 (± 0.055)	-0.329	-0.193	0.108	0.07	0.065
34	-0.007 (± 0.066)	-0.07 (± 0.053)	-0.313	-0.166	0.097	0.175	0.062
40	-0.004 (± 0.056)	-0.064 (± 0.05)	-0.253	-0.186	0.086	0.317	0.06
48	0 (± 0.047)	-0.063 (± 0.047)	0.108	-0.212	0.084	0.305	0.063
56	0.001 (± 0.051)	-0.051 (± 0.054)	-0.159	-0.232	0.08	0.284	0.053
66	0.006 (± 0.052)	-0.036 (± 0.047)	-0.163	-0.187	0.074	0.176	0.042
78	0.008 (± 0.044)	-0.03 (± 0.041)	-0.149	-0.152	0.065	0.191	0.038
92	0.006 (± 0.038)	-0.022 (± 0.041)	-0.113	-0.124	0.057	0.234	0.029
110	0.005 (± 0.031)	-0.014 (± 0.032)	-0.075	-0.096	0.043	0.274	0.019
Spring							
2	0.173 (± 0.341)	-0.111 (± 0.148)	-0.735	-0.416	0.452	0.166	0.285
4	0.118 (± 0.364)	-0.137 (± 0.147)	0.742	-0.495	0.425	0.396	0.255
6	0.112 (± 0.311)	-0.15 (± 0.145)	0.733	-0.492	0.384	0.46	0.263
8	0.024 (± 0.143)	-0.149 (± 0.14)	-0.406	-0.49	0.228	0.454	0.174
10	0.016 (± 0.095)	-0.146 (± 0.137)	0.367	-0.488	0.206	0.414	0.162
12	-0.079 (± 0.131)	-0.141 (± 0.134)	-0.456	-0.486	0.168	0.318	0.062
14	-0.085 (± 0.13)	-0.138 (± 0.13)	-0.498	-0.484	0.162	0.319	0.053
16	-0.075 (± 0.123)	-0.135 (± 0.125)	-0.493	-0.482	0.159	0.304	0.06
18	-0.065 (± 0.114)	-0.124 (± 0.111)	-0.473	-0.478	0.149	0.262	0.059
22	-0.049 (± 0.097)	-0.108 (± 0.096)	-0.427	-0.468	0.135	0.194	0.058
26	-0.04 (± 0.085)	-0.095 (± 0.084)	-0.357	-0.422	0.119	0.228	0.055
30	-0.03 (± 0.076)	-0.086 (± 0.073)	-0.276	-0.336	0.105	0.272	0.055
34	-0.021 (± 0.069)	-0.077 (± 0.064)	-0.242	-0.299	0.095	0.299	0.055

Depth (m)	Mean (± SD) ADCP	Mean (± SD) Mercator data product	Max ADCP	Max Mercator data product	RMSE	ρ	bias
40	-0.013 (± 0.062)	-0.069 (± 0.06)	-0.216	-0.227	0.089	0.295	0.055
48	-0.007 (± 0.058)	-0.066 (± 0.063)	0.174	-0.239	0.09	0.322	0.058
56	-0.003 (± 0.059)	-0.054 (± 0.065)	0.18	-0.239	0.092	0.204	0.051
66	0 (± 0.058)	-0.04 (± 0.062)	0.199	-0.211	0.085	0.183	0.04
78	0.002 (± 0.052)	-0.031 (± 0.062)	0.221	-0.192	0.079	0.149	0.033
92	0.006 (± 0.045)	-0.02 (± 0.059)	0.169	-0.186	0.067	0.271	0.026
110	0.007 (± 0.035)	-0.012 (± 0.039)	-0.16	0.111	0.045	0.396	0.02

Appendix 2. Seasonal statistical comparison between in situ (ADCP) and modelled (Mercator data product) meridional currents (m/s) for all depth bins. Mean (± standard deviation) and greatest current vector (Max) for the ADCP and the Mercator data product data, root-mean-square-error

Depth (m)	Mean (± SD) ADCP	Mean (± SD) Mercator data product	Max ADCP	Max Mercator data product	RMSE	ρ	bias
Summer							
2	0.234 (± 0.381)	0.094 (± 0.108)	0.741	0.349	0.392	0.267	0.14
4	0.033 (± 0.165)	0.045 (± 0.074)	0.224	0.138	0.183	-0.19	-0.011
6	0.284 (± 0.349)	0.091 (± 0.113)	0.729	0.417	0.385	0.222	0.193
8	0.276 (± 0.194)	0.086 (± 0.113)	0.708	0.413	0.279	0.208	0.19
10	0.075 (± 0.077)	0.071 (± 0.11)	0.432	0.315	0.11	0.383	0.003
12	0.067 (± 0.123)	0.071 (± 0.111)	0.382	0.399	0.134	0.369	-0.004
14	0.024 (± 0.119)	0.062 (± 0.113)	0.392	0.389	0.133	0.408	-0.038
16	0.019 (± 0.101)	0.052 (± 0.109)	0.331	0.38	0.129	0.301	-0.033
18	0.015 (± 0.09)	0.048 (± 0.097)	0.29	0.296	0.121	0.226	-0.033
22	-0.003 (± 0.079)	0.051 (± 0.087)	0.213	0.295	0.123	0.111	-0.054
26	-0.019 (± 0.073)	0.05 (± 0.077)	-0.187	0.269	0.121	0.12	-0.069
30	-0.028 (± 0.068)	0.047 (± 0.074)	-0.187	0.266	0.12	0.155	-0.076

Depth (m)	Mean (± SD) ADCP	Mean (± SD) Mercator data product	Max ADCP	Max Mercator data product	RMSE	ρ	bias
34	-0.032 (± 0.064)	0.036 (± 0.072)	-0.179	0.279	0.107	0.266	-0.069
40	-0.035 (± 0.061)	0.027 (± 0.06)	-0.176	0.208	0.092	0.338	-0.062
48	-0.036 (± 0.059)	0.021 (± 0.054)	-0.191	0.175	0.083	0.398	-0.057
56	-0.039 (± 0.058)	0.002 (± 0.062)	-0.206	0.153	0.077	0.408	-0.042
66	-0.042 (± 0.056)	-0.015 (± 0.057)	-0.186	-0.181	0.068	0.349	-0.026
78	-0.045 (± 0.053)	-0.03 (± 0.059)	-0.171	-0.208	0.064	0.392	-0.015
92	-0.046 (± 0.048)	-0.032 (± 0.053)	-0.162	-0.196	0.05	0.571	-0.014
110	-0.046 (± 0.05)	-0.023 (± 0.048)	-0.148	-0.145	0.051	0.556	-0.023
Autumn							
2	0.155 (± 0.35)	0.09 (± 0.088)	0.737	0.357	0.351	0.169	0.064
4	0.05 (± 0.325)	0.092 (± 0.064)	0.642	0.211	0.319	0.144	-0.042
6	0.094 (± 0.334)	0.073 (± 0.079)	0.732	0.282	0.347	-0.092	0.02
8	0.23 (± 0.237)	0.09 (± 0.089)	0.735	0.333	0.284	0.117	0.139
10	0.06 (± 0.07)	0.08 (± 0.087)	0.38	0.33	0.109	0.08	-0.019
12	0.043 (± 0.109)	0.082 (± 0.09)	0.427	0.326	0.142	0.073	-0.038
14	-0.008 (± 0.097)	0.075 (± 0.086)	0.305	0.321	0.155	-0.005	-0.084
16	-0.011 (± 0.089)	0.07 (± 0.084)	-0.243	0.312	0.146	0.021	-0.082
18	-0.017 (± 0.084)	0.065 (± 0.077)	-0.211	0.279	0.137	0.089	-0.082
22	-0.026 (± 0.077)	0.068 (± 0.069)	-0.217	0.253	0.134	0.154	-0.094
26	-0.033 (± 0.067)	0.069 (± 0.064)	-0.234	0.251	0.13	0.229	-0.102
30	-0.035 (± 0.063)	0.068 (± 0.061)	-0.223	0.229	0.126	0.323	-0.104
34	-0.037 (± 0.061)	0.067 (± 0.062)	-0.19	0.277	0.125	0.365	-0.104
40	-0.038 (± 0.059)	0.062 (± 0.058)	-0.221	0.284	0.121	0.361	-0.101
48	-0.041 (± 0.058)	0.06 (± 0.055)	-0.201	0.26	0.118	0.431	-0.101
56	-0.041 (± 0.056)	0.057 (± 0.059)	-0.202	0.241	0.117	0.416	-0.099
66	-0.041 (± 0.054)	0.046 (± 0.052)	-0.191	0.194	0.107	0.379	-0.088
78	-0.041 (± 0.053)	0.035 (± 0.053)	-0.201	0.177	0.098	0.351	-0.076
92	-0.04 (± 0.048)	0.038 (± 0.057)	-0.19	0.21	0.094	0.512	-0.078

Depth (m)	Mean (± SD) ADCP	Mean (± SD) Mercator data product	Max ADCP	Max Mercator data product	RMSE	ρ	bias
110	-0.037 (± 0.048)	0.035 (± 0.05)	-0.141	0.165	0.083	0.638	-0.072
Winter							
2	0.023 (± 0.464)	0.118 (± 0.126)	0.727	0.425	0.456	0.176	-0.094
4	0.212 (± 0.468)	0.1 (± 0.117)	0.731	0.396	0.484	-0.047	0.111
6	0.175 (± 0.469)	0.077 (± 0.109)	0.742	0.344	0.473	0.088	0.097
8	0.145 (± 0.281)	0.07 (± 0.116)	-0.582	0.326	0.32	-0.127	0.074
10	0.087 (± 0.089)	0.068 (± 0.114)	0.32	0.312	0.139	0.082	0.018
12	0.026 (± 0.106)	0.065 (± 0.111)	0.333	0.31	0.137	0.269	-0.038
14	0.014 (± 0.102)	0.06 (± 0.105)	0.304	0.307	0.132	0.288	-0.046
16	0.012 (± 0.099)	0.055 (± 0.097)	0.298	0.317	0.121	0.33	-0.042
18	0.013 (± 0.096)	0.058 (± 0.076)	0.303	0.286	0.109	0.322	-0.044
22	0.013 (± 0.091)	0.07 (± 0.062)	0.288	0.251	0.111	0.282	-0.057
26	0.013 (± 0.087)	0.08 (± 0.061)	0.273	0.215	0.118	0.17	-0.066
30	0.014 (± 0.079)	0.081 (± 0.064)	0.256	0.21	0.114	0.184	-0.067
34	0.015 (± 0.071)	0.081 (± 0.061)	0.228	0.219	0.1	0.311	-0.066
40	0.018 (± 0.065)	0.077 (± 0.057)	0.206	0.218	0.082	0.487	-0.059
48	0.016 (± 0.061)	0.07 (± 0.057)	0.178	0.246	0.076	0.54	-0.053
56	0.011 (± 0.065)	0.056 (± 0.068)	0.246	0.251	0.074	0.595	-0.045
66	0.007 (± 0.066)	0.036 (± 0.058)	0.263	0.2	0.063	0.585	-0.029
78	0.005 (± 0.062)	0.029 (± 0.053)	0.236	0.192	0.059	0.555	-0.024
92	0.006 (± 0.061)	0.037 (± 0.057)	0.233	0.226	0.056	0.68	-0.031
110	0.007 (± 0.057)	0.033 (± 0.049)	0.181	0.193	0.043	0.782	-0.025
Spring							
2	0.19 (± 0.397)	0.096 (± 0.146)	0.74	0.44	0.409	0.192	0.094
4	0.279 (± 0.432)	0.12 (± 0.142)	0.748	0.436	0.458	0.186	0.159
6	0.296 (± 0.417)	0.113 (± 0.126)	-0.749	0.43	0.46	0.063	0.182
8	0.202 (± 0.25)	0.109 (± 0.115)	0.652	0.427	0.285	0.059	0.092
10	0.116 (± 0.104)	0.104 (± 0.112)	0.392	0.424	0.136	0.185	0.012

Depth (m)	Mean (± SD) ADCP	Mean (± SD) Mercator data product	Max ADCP	Max Mercator data product	RMSE	ρ	bias
12	0.075 (± 0.127)	0.098 (± 0.11)	-0.37	0.421	0.157	0.121	-0.023
14	0.061 (± 0.12)	0.094 (± 0.107)	-0.337	0.418	0.157	0.067	-0.032
16	0.057 (± 0.115)	0.089 (± 0.102)	-0.32	0.414	0.152	0.048	-0.032
18	0.054 (± 0.111)	0.085 (± 0.091)	0.316	0.408	0.145	0.021	-0.03
22	0.048 (± 0.101)	0.083 (± 0.084)	0.324	0.392	0.132	0.087	-0.035
26	0.043 (± 0.092)	0.082 (± 0.079)	0.284	0.297	0.116	0.215	-0.039
30	0.039 (± 0.088)	0.079 (± 0.075)	0.265	0.291	0.102	0.341	-0.04
34	0.035 (± 0.086)	0.079 (± 0.075)	0.25	0.297	0.096	0.425	-0.044
40	0.03 (± 0.083)	0.076 (± 0.072)	0.268	0.289	0.091	0.476	-0.046
48	0.02 (± 0.082)	0.072 (± 0.074)	0.26	0.279	0.092	0.504	-0.052
56	0.009 (± 0.083)	0.06 (± 0.081)	-0.229	0.264	0.096	0.485	-0.05
66	0 (± 0.078)	0.039 (± 0.073)	-0.216	0.21	0.086	0.474	-0.04
78	-0.008 (± 0.075)	0.025 (± 0.067)	-0.224	0.19	0.08	0.462	-0.034
92	-0.009 (± 0.071)	0.032 (± 0.073)	0.234	0.23	0.076	0.597	-0.041
110	-0.008 (± 0.069)	0.032 (± 0.064)	0.193	0.191	0.061	0.759	-0.041

Appendix 3. Pseudo code from R studio

```
rm(list=ls())
setwd("C:/Users/Dell/OneDrive - University of Cape Town/University/2023/Thesis/Stats")

#Input and organise ADCP data ----
adcp_raw_uv <- read.csv('ADCP_Raw_UV.csv')

adcp_raw_uv$DateTime <- as.POSIXct(adcp_raw_uv$DateTime, format='%m/%d/%Y %H:%M:%S')  #set date time format
adcp_raw_uv <- adcp_raw_uv[adcp_raw_uv$Pressure > 110,]  #subset to only when its in the sea
colnames(adcp_raw_uv) <- read.csv('adcp uv headings.csv', header = F)  #rename columns
adcp_raw_uv[adcp_raw_uv == -32.768] <- NA

#rolling mean
library(zoo)
adcp_rolling_uv <- adcp_raw_uv
adcp_rolling_uv[3:124] <- rollmean(adcp_rolling_uv[3:124], 12, fill=NA, align = 'right') #calculate a right aligned (previous) rolling mean, using 12 half hour slots so 6 hours
```

```
#select only comparable depths
adcp_rolling_uv<- subset(adcp_rolling_uv, sel = c(1, 2, 13, 14, 31, 32, 45, 46, 57, 58, 67, 68, 75, 76, 83, 84, 89, 90, 93, 94, 97, 98, 101, 102, 105:122))

#Wide to long
library(tidyr)
adcp_u <- pivot_longer(data = adcp_rolling_uv, cols = seq(3, 42, by = 2), names_to = 'depth', values_to = 'U')
adcp_u <- subset(adcp_u, select = -c(2:22))     #remove the V columns from the subset
adcp_u$depth <- gsub('mU', '', adcp_u$depth)    #remove the letters from the column so they merge properly

adcp_v <- pivot_longer(data = adcp_rolling_uv, cols = seq(4, 42, by = 2), names_to = 'depth', values_to = 'V')
adcp_v <- subset(adcp_v, select = -c(2:22))     #remove the U columns from the subset
adcp_v$depth <- gsub('mV', '', adcp_v$depth)    #remove the letters from the column so they merge properly

adcp_uv_rol_long <- merge(adcp_u, adcp_v, by = c('time', 'depth'))

#speed direction just for consistency
adcp_uv_rol_long$speed <- sqrt(adcp_uv_rol_long$V^2 + adcp_uv_rol_long$U^2)
adcp_uv_rol_long$dir  <-  ((atan2(adcp_uv_rol_long$V,  adcp_uv_rol_long$U))*180/pi)  %% 360

adcp_uv_rol_long$depth <- as.numeric(adcp_uv_rol_long$depth)
summary(adcp_uv_rol_long)

#round date to nearest half hour
library(lubridate)
adcp_uv_rol_long$time  <-  round_date(adcp_uv_rol_long$time,  unit  =  '30  minutes')  #removes the parts of the data set that have 59 seconds on the end

#Input cmemcs data ----
cmems <- read.csv2('cmems_mod_glo_phy-cur_anfc_0.083deg_PT6H-i_2022_2023.csv')
cmems$time <- as.POSIXct(cmems$time, format='%Y-%m-%d %H:%M:%S')
cmems[,c(1,2,3,5,6)]  <-  apply(cmems[,c(1,2,3,5,6)],  2,  function(x) as.numeric(as.character(x)))
cmems$speed <- sqrt(cmems$nsv.m.s.^2 + cmems$esv.m.s.^2)
cmems$dir <- ((atan2(cmems$nsv.m.s., cmems$esv.m.s.))*180/pi) %% 360

#remove lat and lon columns
library(dplyr)
cmems <- select(cmems, select = -c('lat', 'lon'))

#cut and rename cmems depths to match adcp depths
```

```
cmems <- cmems[!(cmems$depth %in% c(0.494025, 1.541375, 5.078224, 130.666000, 155.850693)),]
values_to_replace <- c(2.645669, 3.819495, 6.440614, 7.929560, 9.572997, 11.405000, 13.467140, 15.810070, 18.495560, 21.598820, 25.211411, 29.444731, 34.434151, 40.344051, 47.373692, 55.764290, 65.807266, 77.853851, 92.326073, 109.729301)
replacements <- c(2, 4, 6, 8, 10, 12, 14, 16, 18, 22, 26, 30, 34, 40, 48, 56, 66, 78, 92, 110)
cmems$depth[cmems$depth %in% values_to_replace] <- replacements[match(cmems$depth, values_to_replace)]
summary(cmems)

#merged data set and saved as csv ----
cmems_adcp <- merge(adcp_uv_rol_long, cmems, by = c('depth', 'time'))        #make one combined dataset for complete time match
cmems_adcp <- select(cmems_adcp, -c('speed.x', 'dir.x', 'speed.y', 'dir.y'))  #remove excess columns
write.csv(cmems_adcp, 'C:/Users/Dell/OneDrive - University of Cape Town/University/2023/Thesis/Stats/cmems_adcp_UV_code.csv', row.names=FALSE)

cmems_full_adcp <- merge(adcp_uv_rol_long, cmems, by = c('depth', 'time'), all.y = T) #make one combined dataset with the full mercator data
cmems_full_adcp <- select(cmems_full_adcp, -c('speed.x', 'dir.x', 'speed.y', 'dir.y'))
write.csv(cmems_full_adcp, 'C:/Users/Dell/OneDrive - University of Cape Town/University/2023/Thesis/Stats/cmems_full_adcp_UV_code.csv', row.names=FALSE)

#CODE CAN START FROM HERE!!!----
cmems_adcp <- read.csv('cmems_adcp_UV_code.csv')
cmems_adcp <- subset(cmems_adcp, cmems_adcp[,3] > -0.75 & cmems_adcp[,4] > -0.75) #remove all erronious values
cmems_adcp <- subset(cmems_adcp, cmems_adcp[,3] < 0.75 & cmems_adcp[,4] < 0.75) #remove all erronious values
cmems_adcp <- na.omit(cmems_adcp)
cmems_adcp$time <- as.POSIXct(cmems_adcp$time, format='%Y-%m-%d %H:%M:%S')
summary(cmems_adcp)

library(lubridate)
unique(month(cmems_adcp$time))


#mean and sd ----
library(dplyr)
adcp_uv_mean_sd <- cmems_adcp %>% group_by(depth) %>%
  summarise(mean_u_adcp = mean(U, na.rm = TRUE),
            mean_v_adcp = mean(V, na.rm = TRUE),
            sd_u_adcp = sd(U, na.rm = TRUE),
            sd_v_adcp = sd(V, na.rm = TRUE),
            min_u_adcp = min(U, na.rm = TRUE),
            min_v_adcp = min(V, na.rm = TRUE),
```

```
        max_u_adcp = max(U, na.rm = TRUE),
        max_v_adcp = max(V, na.rm = TRUE))

cmems_mean_sd <- cmems_adcp %>% group_by(depth) %>%
  summarise(mean_u_cmems = mean(esv.m.s..U., na.rm = TRUE),
        mean_v_cmems = mean(nsv.m.s..V., na.rm = TRUE),
        sd_u_cmems = sd(esv.m.s..U., na.rm = TRUE),
        sd_v_cmems = sd(nsv.m.s..V., na.rm = TRUE),
        min_u_cmems = min(esv.m.s..U., na.rm = TRUE),
        min_v_cmems = min(nsv.m.s..V., na.rm = TRUE),
        max_u_cmems = max(esv.m.s..U., na.rm = TRUE),
        max_v_cmems = max(nsv.m.s..V., na.rm = TRUE))

#RMSE ----
#U
rmse_u <- function(data, depth_value) {
  subset_data <- data[data$depth == depth_value, ]
  subset_data <- subset_data[complete.cases(subset_data), ]
  if(nrow(subset_data) > 0) {
    rmse <- sqrt(mean((subset_data$U - subset_data$esv.m.s..U.)^2))
    return(rmse)
  } else {
    return(NA)
  }
}

#V
rmse_v <- function(data, depth_value) {
  subset_data <- data[data$depth == depth_value, ]
  subset_data <- subset_data[complete.cases(subset_data), ]
  if(nrow(subset_data) > 0) {
    rmse <- sqrt(mean((subset_data$V - subset_data$nsv.m.s..V.)^2))
    return(rmse)
  } else {
    return(NA)
  }
}

rmse <- merge(data.frame(depth = unique(cmems_adcp$depth), rmse_u =
sapply(unique(cmems_adcp$depth), function(depth_val) {
  rmse_u(cmems_adcp, depth_val)
})), data.frame(depth = unique(cmems_adcp$depth), rmse_v =
sapply(unique(cmems_adcp$depth), function(depth_val) {
  rmse_v(cmems_adcp, depth_val)
})), by = 'depth')

#spearman correlation ----
```

```
spear_u <- function(data, depth_value) {
  subset_data <- data[data$depth == depth_value, ]
  subset_data <- subset_data[complete.cases(subset_data), ]
  if (nrow(subset_data) >0) {
    r_squared <- cor(subset_data$U, subset_data$esv.m.s..U., method = 'spearman')
    return(r_squared)
  } else {
    return(NA)
  }
}

spear_v <- function(data, depth_value) {
  subset_data <- data[data$depth == depth_value, ]
  subset_data <- subset_data[complete.cases(subset_data), ]
  if (nrow(subset_data) >0) {
    r_squared <- cor(subset_data$V, subset_data$nsv.m.s..V., method = 'spearman')
    return(r_squared)
  } else {
    return(NA)
  }
}

spear <- merge(data.frame(depth = unique(cmems_adcp$depth), spear_u =
sapply(unique(cmems_adcp$depth), function(depth_val) {
  spear_u(cmems_adcp, depth_val)
})), data.frame(depth = unique(cmems_adcp$depth), spear_v =
sapply(unique(cmems_adcp$depth), function(depth_val) {
  spear_v(cmems_adcp, depth_val)
})), by = 'depth')


#bias ----
bias_u <- function(data, depth_value) {
  subset_data <- data[data$depth == depth_value, ]
  subset_data <- subset_data[complete.cases(subset_data), ]
  if (nrow(subset_data) >0) {
    bias <- mean(subset_data$U - subset_data$esv.m.s..U.)
    return(bias)
  } else {
    return(NA)
  }
}

bias_v <- function(data, depth_value) {
  subset_data <- data[data$depth == depth_value, ]
  subset_data <- subset_data[complete.cases(subset_data), ]
  if (nrow(subset_data) >0) {
```

```
  bias <- mean(subset_data$V - subset_data$nsv.m.s..V.)
  return(bias)
 } else {
  return(NA)
 }
}

bias <- merge(data.frame(depth = unique(cmems_adcp$depth), bias_u =
sapply(unique(cmems_adcp$depth), function(depth_val) {
 bias_u(cmems_adcp, depth_val)
})), data.frame(depth = unique(cmems_adcp$depth), bias_v =
sapply(unique(cmems_adcp$depth), function(depth_val) {
 bias_v(cmems_adcp, depth_val)
})), by = 'depth')

#Combined stats datasheet ----
results <- merge(adcp_uv_mean_sd, cmems_mean_sd, by = 'depth')
results <- merge(results, rmse, by = 'depth')
results <- merge(results, spear, by = 'depth')
results <- merge(results, bias, by = 'depth')

#save as csv
write.csv(results, 'C:/Users/Dell/OneDrive - University of Cape
Town/University/2023/Thesis/Stats/results.csv', row.names = T)

#Season split ----
library(lubridate)
library(dplyr)
cmems_adcp$season <- if_else(month(cmems_adcp$time) %in% c(12, 1, 2), 'Summer',
                    if_else(month(cmems_adcp$time) %in% c(3, 4, 5), 'Autum',
                         if_else(month(cmems_adcp$time) %in% c(6, 7, 8), 'Winter',
                              if_else(month(cmems_adcp$time) %in% c(9, 10, 11),'Spring',""))))

#test for normality ----
par(mfrow = c(2,2))

hist(cmems_adcp$U, breaks = 70, main = "", xlab = 'Zonal ADCP (m/s)', prob = T, xlim = c(-0.4,
0.6), ylim = c(0, 14))
curve(dnorm(x, mean = mean(cmems_adcp$U), sd = sd(cmems_adcp$U)), col="red", lwd=1,
add=TRUE, yaxt="n")
hist(cmems_adcp$V, breaks = 100, main = "", xlab = 'Meridional ADCP (m/s)', prob = T, xlim =
c(-0.4, 0.6), ylim = c(0, 14))
curve(dnorm(x, mean = mean(cmems_adcp$V), sd = sd(cmems_adcp$V)), col="red", lwd=1,
add=TRUE, yaxt="n")
hist(cmems_adcp$esv.m.s..U., breaks = 25, main = "", xlab = 'Zonal Mercator (m/s)', prob = T,
xlim = c(-0.4, 0.6), ylim = c(0, 14))
```

```
curve(dnorm(x, mean = mean(cmems_adcp$esv.m.s..U.), sd = sd(cmems_adcp$esv.m.s..U.)),
col="red", lwd=1, add=TRUE, yaxt="n")
hist(cmems_adcp$nsv.m.s..V., breaks = 25, main = "", xlab = 'Meridional Mercator (m/s)',
prob = T, xlim = c(-0.4, 0.6), ylim = c(0, 14))
curve(dnorm(x, mean = mean(cmems_adcp$nsv.m.s..V.), sd = sd(cmems_adcp$nsv.m.s..V.)),
col="red", lwd=1, add=TRUE, yaxt="n")
par(mfrow = c(1,1))

library(ggpubr)
install.packages('cowplot')
library(cowplot)
plot_grid(qqnorm(cmems_adcp$U),
        qqnorm(cmems_adcp$V),
        qqnorm(cmems_adcp$esv.m.s..U.),
        qqnorm(cmems_adcp$nsv.m.s..V.))     #the data are not normal

qqplot(cmems_adcp$esv.m.s..U., cmems_adcp$U)

library(nortest)
ad.test(cmems_adcp$nsv.m.s..V.)
library(moments)
skewness(cmems_adcp$nsv.m.s..V., na.rm = T)
kurtosis(cmems_adcp$nsv.m.s..V., na.rm = T)


#Plot ADCP vs cmems on one axis, one plot per depth ----
cmems_adcp_no_na <- na.omit(cmems_adcp)
depth_values <- unique(cmems_adcp_no_na$depth)
for (depth_value in depth_values) {
  subset_data <- cmems_adcp_no_na[cmems_adcp_no_na$depth == depth_value, ]
  max_range_U <- max(range(subset_data$U), range(subset_data$esv.m.s..U.))
  max_range_V <- max(range(subset_data$V), range(subset_data$nsv.m.s..V.))
  min_range_U <- min(range(subset_data$U), range(subset_data$esv.m.s..U.))
  min_range_V <- min(range(subset_data$V), range(subset_data$nsv.m.s..V.))
  plot(subset_data$U, subset_data$esv.m.s..U., main = paste("U Depth =", depth_value), xlab
= "ADCP", ylab = "CMEMS", xlim = c(min_range_U, max_range_U), ylim = c(min_range_U,
max_range_U))
  abline(a=0, b=1)
  plot(subset_data$V, subset_data$nsv.m.s..V., main = paste("V Depth =", depth_value), xlab
= "ADCP", ylab = "CMEMS", xlim = c(min_range_V, max_range_V), ylim = c(min_range_V,
max_range_V))
  abline(a=0, b=1)
}



#Plot comparison full time series  ----
```

```
depth_values <- unique(cmems_adcp$depth)
monthly_ticks <- seq(as.POSIXct('2022-11-01 00:00:00', format = '%Y-%m-%d %H:%M:%S'), as.POSIXct('2023-12-01 12:00:00', format = '%Y-%m-%d %H:%M:%S'), by = 'months' )

for (depth_value in depth_values) {
  subset_data <- cmems_adcp_no_na[cmems_adcp_no_na$depth == depth_value, ]

  png(paste('U', depth_value, '.png', sep = ''), width = 1500, height = 400)
  par(mar = c(5,5,1,1))
  plot(subset_data$esv.m.s..U. ~ subset_data$time, type = 'l', ylim = c(-0.6, 0.6), col = 'black', xlab = 'Time', ylab = paste('Zonal current vector (m/s) at', depth_value, 'm'), xaxt = 'n', cex.axis = 1.5, cex.lab = 1.5)
  lines(subset_data$U ~ subset_data$time, type = 'l', col = 'red', new = F)
  axis(1, at = monthly_ticks, labels = format(monthly_ticks, '%b %Y'), cex.axis = 1.5, las =0)
  legend('topright', legend = c('Mercator', 'ADCP'), col = c('black', 'red'), lty = 1, bty = 'n', cex = 1.5, lwd = 2)
  abline(h = c(-0.2, 0.2, -0.4, 0.4), lty = 2)
  abline(h = 0, v = c(monthly_ticks[c(2, 5, 8, 11)]), lty = 1, lwd = 0.5, col = 'grey')
  dev.off()

  png(paste('V', depth_value, '.png', sep = ''), width = 1500, height = 400)
  par(mar = c(5,5,1,1))
  plot(subset_data$nsv.m.s..V. ~ subset_data$time, type = 'l', ylim = c(-0.6, 0.6), col = 'black', xlab = 'Time', ylab = paste('Meridional current vector (m/s) at', depth_value, 'm'), xaxt = 'n', cex.axis = 1.5, cex.lab = 1.5)
  lines(subset_data$V ~ subset_data$time, type = 'l', col = 'red', new = F)
  axis(1, at = monthly_ticks, labels = format(monthly_ticks, '%b %Y'), cex.axis = 1.5, las =0)
  legend('topright', legend = c('Mercator', 'ADCP'), col = c('black', 'red'), lty = 1, bty = 'n', cex = 1.5, lwd = 2)
  abline(h = c(-0.2, 0.2, -0.4, 0.4), lty = 2)
  abline(h = 0, v = c(monthly_ticks[c(2, 5, 8, 11)]), lty = 1, lwd = 0.5, col = 'grey')
  dev.off()
}
#Plot comparison full time series  with full mercator----
cmems_full_adcp <- read.csv('cmems_full_adcp_UV_code.csv')
cmems_full_adcp$time <- as.POSIXct(cmems_full_adcp$time, format='%Y-%m-%d %H:%M:%S')

unique(month(cmems_full_adcp$time))

for (depth_value in depth_values) {
  subset_data <- cmems_full_adcp[cmems_full_adcp$depth == depth_value, ]

  png(paste('Ufull', depth_value, '.png', sep = ''), width = 1500, height = 400)
  par(mar = c(5,5,1,1))
```

```
  plot(subset_data$esv.m.s..U. ~ subset_data$time, type = 'l', ylim = c(-0.6, 0.6), col = 'black',
xlab = 'Time', ylab = paste('Zonal current vector (m/s) at', depth_value, 'm'), xaxt = 'n', cex.axis
= 1.5, cex.lab = 1.5)
  abline(h=0, lty = 1, col = 'black')
  lines(subset_data$U ~ subset_data$time, type = 'l', col = 'red', new = F)
  axis(1, at = monthly_ticks, labels = format(monthly_ticks, '%b %Y'), cex.axis = 1.5, las =0)
  legend('topright', legend = c('Mercator', 'ADCP'), col = c('black', 'red'), lty = 1, bty = 'n', cex =
1.5, lwd = 2)
  abline(h = c(-0.2, 0.2, -0.4, 0.4), lty = 2)
  abline(v = c(monthly_ticks[c(2, 5, 8, 11)]), lty = 1, lwd = 0.5, col = 'grey')
  dev.off()

  png(paste('Vfull', depth_value, '.png', sep = ''), width = 1500, height = 400)
  par(mar = c(5,5,1,1))
  plot(subset_data$nsv.m.s..V. ~ subset_data$time, type = 'l', ylim = c(-0.6, 0.6), col = 'black',
xlab = 'Time', ylab = paste('Meridional current vector (m/s) at', depth_value, 'm'), xaxt = 'n',
cex.axis = 1.5, cex.lab = 1.5)
  abline(h=0, lty=1, col = 'black')
  lines(subset_data$V ~ subset_data$time, type = 'l', col = 'red', new = F)
  axis(1, at = monthly_ticks, labels = format(monthly_ticks, '%b %Y'), cex.axis = 1.5, las =0)
  legend('topright', legend = c('Mercator', 'ADCP'), col = c('black', 'red'), lty = 1, bty = 'n', cex =
1.5, lwd = 2)
  abline(h = c(-0.2, 0.2, -0.4, 0.4), lty = 2)
  abline(v = c(monthly_ticks[c(2, 5, 8, 11)]), lty = 1, lwd = 0.5, col = 'grey')
  dev.off()
}
t <- subset(cmems_adcp_no_na, depth == 110)
```